EXPERIMENTAL STUDIES OF PHOTOIONIZATION PROCESSES IN AIR

Walter H. Wurster, et al

Calspan Corporation

Prepared for:

Office of Naval Research
Advanced Research Projects Agency

October 1973

AD-768 913

Calspan

On November 17, 1972 Cornell Aeronautical Laboratory (CAL) changed its name to Calspan Corporation end converted to for-profit operations. Calspan is dedicated to carrying on CAL's long-standing tradition of advenced research and development from an independent viewpoint. All of CAL's diverse sclentific and engineering programs for government and industry are being continued in the aarosciences, electronics and avionics, computer sciences, transportation and vehicle research, end the environmental sclerces. Calspan is composed of the same staff, management, and facilities as CAL, which oparated since 1946 under faderal income tax exemption.

EXPERIMENTAL STUDIES OF PHOTOIONIZATION PROCESSES IN AIR

P.V. Marrone, T.M. Albrechcinski and W.H. Wurster

FINAL TECHNICAL REPORT

Calspan Report No. AI-3107-A-4

October 1973

Principal Investigator:	Dr. Walter H. Wurster (716) 632-7500 Calspan Corporation
Scientific Officer:	Director, Physics Program Physical Sciences Division, Office of Naval Research Arlington, Virginia 22217
Contract No.:	N00014-71-C-0387
Effective Date of Contract:	1 May 1971
Contract Expiration Date:	31 October 1973
Amount of Contract:	$100,744

Sponsored By:

ADVANCED RESEARCH PROJECTS AGENCY
ARPA ORDER NO. 1479, AMENDMENT NO. 3/3-11-71
PROGRAM CODE NO. 000001E20K21

UNCLASSIFIED

SECURITY CLASSIFICATION OF THIS PAGE (When Data Entered)

REPORT DOCUMENTATION PAGE		READ INSTRUCTIONS BEFORE COMPLETING FORM
1. REPORT NUMBER	2. GOVT ACCESSION NO.	3. RECIPIENT'S CATALOG NUMBER
4. TITLE (and Subtitle) EXPERIMENTAL STUDIES OF PHOTOIONIZATION PROCESSES IN AIR		5. TYPE OF REPORT & PERIOD COVERED Final Technical Report 5/1/71 - 8/31/73
		6. PERFORMING ORG. REPORT NUMBER AI ~~3017-A-4~~ 3107-A-4
7. AUTHOR(s) Paul V. Marrone, Thomas M. Albrechcinski, Walter H. Wurster		8. CONTRACT OR GRANT NUMBER(s) N00014-71-C-0387
9. PERFORMING ORGANIZATION NAME AND ADDRESS Calspan Corporation 4455 Genesee Street Buffalo, New York 14221		10. PROGRAM ELEMENT, PROJECT, TASK AREA & WORK UNIT NUMBERS 000001E20K21
11. CONTROLLING OFFICE NAME AND ADDRESS Director, Physics Program, Physical Sciences Division - Office of Naval Research 800 North Quincy Street, Arlington, Va. 22217		12. REPORT DATE October, 1973 13. NUMBER OF PAGES 58
14. MONITORING AGENCY NAME & ADDRESS(if different from Controlling Office)		15. SECURITY CLASS. (of this report) Unclassified 15a. DECLASSIFICATION DOWNGRADING SCHEDULE N/A

16. DISTRIBUTION STATEMENT (of this Report)

Unlimited distribution

17. DISTRIBUTION STATEMENT (of the abstract entered in Block 20, if different from Report)

18. SUPPLEMENTARY NOTES

19. KEY WORDS (Continue on reverse side if necessary and identify by block number)

(1) Shock-induced radiation (2) vacuum UV radiation, (3) shock tube experiments, (4) absorption and excitation measurements, (5) windowless wavelength region, (6) sidewall and endwall radiation.

20. ABSTRACT (Continue on reverse side if necessary and identify by block number)

The radiative properties of shock-heated gases are much different from those measured at standard conditions and extrapolations to nonequilibrium situations cannot be readily made. Under strong shock conditions, vibrational and rotational excited states of the molecular species are populated in nonequilibrium distributions, where different temperatures must be assigned to each of the internal energy modes. Examples of this are found in such areas as reentry physics and nuclear blast effects.

DD FORM 1 JAN 73 1473 EDITION OF 1 NOV 65 IS OBSOLETE

UNCLASSIFIED

SECURITY CLASSIFICATION OF THIS PAGE (When Data Entered)

Preceding page blank

The experimental program described herein was designed to investigate vacuum ultraviolet radiation processes in air, with particular emphasis directed at the interaction of shock-induced nonequilibrium radiation with gaseous species. The program was divided into three main tasks which were:

1) To perform [NO] absorption measurements using a shock-tube splitter plate technique.

2) To investigate VUV excitation mechanisms utilizing sidewall radiation overshoot measurements.

3) To perform endwall radiation measurements of the advancing shock front to verify previously developed excitation and radiative flux models.

The results of this program are summarized.

TECHNICAL REPORT SUMMARY

Technical Problem:

An experimental program to investigate basic vacuum ultraviolet photoionization processes in air has recently been completed at Calspan Corporation. Particular emphasis was directed toward the interaction of shock-induced nonequilibrium radiation with gaseous species.

The methodology involved the following approach:

1. Perform quantitative measurements to determine the contribution of the NO molecule to the nonequilibrium, vacuum ultraviolet emission spectrum from shock-heated air.
2. Obtain quantitative, spectrally resolved measurements of the nonequilibrium, vacuum ultraviolet flux from advancing shock waves to verify previously developed excitation and radiative flux models.
3. Investigate possible excitation mechanisms leading to VUV emission from molecular species pertinent to high-altitude rocket plume radiation.

Technical Results:

Experiments have been carried out pertinent to all three of the above areas. The splitter-plate absorption technique was utilized to investigate the role of NO in defining shock-induced vacuum ultraviolet radiative flux. Shock radiation measurements using the splitter-plate technique for absorption were obtained at selected wavelengths over a broad wavelength interval, 706 Å $< \lambda <$ 1200 Å, at a resolution of $\Delta\lambda$ = 32 Å. Two test gases were used; a mixture of 10% N_2 + 90% Neon both to confirm previous measurements, and obtain new absorption data for pure N_2 with which to compare data from the total gases; and a 2% N_2 + 8% O_2 + 90% Neon

mixture for absorption measurements in a shocked gaseous mixture containing vibrationally excited NO. The experimental data show substantial absorption at wavelengths 812 Å ⟷ 980 Å for the $N_2/O_2/N_e$ mixture. Computations indicate that much of this absorption can be attributed to the presence of NO in the shocked gas.

A series of experiments were completed with new endwall diagnostics used to view radiation from advancing shock waves. Measurements were obtained both in the VUV and red wavelength regions over a shock velocity range from 14,000-17,000 ft/sec in nitrogen. The 3-channel VUV spectrometer was attached to a new endwall flange in a windowless manner, utilizing the explosively driven plunger. Advancing shock VUV flux data were obtained for selected wavelength intervals, but the low flux level precluded quantative data analysis. More definitive VUV data were obtained over a large bandpass (1050-1800 Å) using an EMR solar-blind PMT.

Modified sidewall optics were installed on the shock tube so as to obtain highly spatially resolved data on the nonequilibrium radiation peak behind incident shock waves for three band systems. These measurements were obtained simultaneously with the endwall data, and covered the same shock velocity range. The time-to-peak radiation for the $N_2(1+)$ red system was observed to be much less than the time-to-peak for the $N_2(4+)$ system in the UV for example.

A discussion of the results obtained for all three tasks is given in Section III.

Comments:

The present document is the final technical report on the experimental studies program. Data were obtained pertinent to all three tasks, and indicated areas in need of further study, such as the role of O atoms on excitation mechanisms, immediate post-shock absorption processes in the vacuum ultraviolet, and the velocity dependence of various radiating band systems were noted.

TABLE OF CONTENTS

I. INTRODUCTION

The radiative properties of shock-heated gases are much different from those measured at standard conditions, and extrapolations to nonequilibrium situations cannot readily be made. Under strong-shock conditions, vibrational and rotational excited states of the molecular species are populated in nonequilibrium distributions, where different temperatures must be assigned to each of the internal energy modes. The calculation of the ionizing radiative flux emerging from a shock-heated gas has been discussed in Ref. 1, and involves a knowledge of the gas dynamics and chemistry of the flow field, the population of the excited states responsible for the radiation, the spectral shape and distribution of the radiation in the wavelength region of interest, and a knowledge of the radiation transfer process, including emission and absorption in the shock-heated gas. Examples of such situations are found in areas of nuclear effects as well as reentry physics. The rate of early fireball growth, for instance, involves the interaction of photons with shocked atmospheric gases.

The experimental research program reported herein is designed to provide data pertinent to vacuum ultraviolet radiation and excitation processes in air. Two of the tasks addressed in the present research program are based on results obtained in the course of a reentry-related research program in which the photoionization of the ambient atmosphere in front of a blunt reentry body was treated.[1, 2, 3] These results were presented in detail in Ref. 1, and will not be discussed here. However, during the course of those experimental studies for N_2 and subsequent computations for air, the question arose as to the contribution of the NO molecule in the determination of the nonequilibrium VUV emissive and absorptive properties of shock-heated air. Based upon available data for cold NO absorption,[5, 6, 7] it may be expected that NO will affect the VUV flux intensity, which highlights the need for absorption coefficient data as a function of temperature. In addition, VUV flux measurements from advancing shock fronts would help to verify previously developed excitation models, and determine the spectral distribution of the radiative flux to compare with predicted values.

The third area of VUV excitation mechanisms pertains not only to shock-induced radiation but is of importance in such areas as high-altitude rocket plume radiation. Thus, nonequilibrium overshoot measurements obtained during the course of the experimental program are directly applicable to the determination of excitation mechanisms.

Section II of this report presents an overall description of the experimental program as well as more detailed discussions of the experimental configurations and results pertinent to each task. A general summary of the experimental measurements is presented in Section III.

II. RESEARCH PROGRAM

In this section a description is presented of the overall experimental configuration used to obtain shock-induced radiation measurements. In addition, detailed presentations are given for specific configurations and diagnostics for separate measurements.

II. 1 DESCRIPTION OF APPARATUS

The shock tube used in these studies was specifically designed for radiation measurements and has been reported earlier (see Refs. 8, 9 and 10 for example). The tube has an internal diameter of 3 inches, with a driver 5 feet in length and a low-pressure section 30 feet long. Room temperature hydrogen was used as the driver gas at pressures ranging from 675-4000 psi for the present series of experiments. The double-diaphragm technique was used to insure repeatability in the shock conditions and mild steel was used as the diaphragm material.

The shock wave speed was monitored over the last 12 feet of the test section with seven thin-film heat transfer gauges mounted along the tube wall. The first two intervals were 3 feet apart, while the last four intervals were 1.5 feet apart, the last station being approximately 1 inch from the reflecting end wall. Megacycle timing counters were used to determine the shock velocity to better than $\pm$ 0.5%.

Between experiments the shock-tube test section was thoroughly scrubbed with alcohol, purged with atmospheric pressure Argon, and hard-pumped with a liquid-nitrogen trapped oil-diffusion pump. Pressure levels of 1-2 x 10^{-5} torr (as indicated by an ionization gauge) were obtained in the test section prior to loading of the test gas. A shock-tube experiment was never undertaken unless this pre-load pressure was less than 2 x 10^{-5} torr. The rate of pressure rise of the entire shock tube and gas-handling system was about 1 μ /hour.

A Baratron differential pressure gauge, capable of measuring pressure in the 0 to 30 torr range with micron precision, was used to control and measure the initial test gas pressure in the shock tube. The ultra-pure

test gases used in these experiments were supplied by Air-Products and Chemicals, Inc. Pure nitrogen, mixtures of nitrogen and neon, and mixtures of nitrogen, oxygen and neon were used as the test gases during various portions of the experimental program.

II.2 EXPERIMENTAL CONFIGURATIONS

The three types of measurements will be discussed in this section of the report: the splitter-plate absorption experiments, the sidewall radiation overshoot measurements, and the endwall-advancing shock wave experiments. Each type of measurement utilized a particular experimental configuration and diagnostic implementation.

II.2.1 Splitter-Plate Absorption Measurements

II.2.1.1 Experiment Definition

A VUV absorption measurement program for the NO molecule, similar in scope to that described in Refs. 1,2 for the N_2 molecule was completed. These measurements were obtained using the high-purity shock tube, with two pertinent features for VUV measurements of this type. The first feature of the experimental arrangement is a 3-channel vacuum ultraviolet spectrometer coupled to the shock tube by an explosively-driven plunger unit, which serves as a fast-acting valve-shutter combination. This windowless plunger was developed under a research program in which photoionization cross sections for N, O, and C were obtained[8, 9, 10] from emission measurements in the windowless region of the vacuum ultraviolet ($\lambda < 1050$ Å). The second feature is a splitter plate which fits into the shock tube at the reflecting wall. The oncoming incident shock is divided and proceeds down two separate channel. One channel is obstructed and the shock is reflected. This pocket of gas serves as the light source (I_o). The light passes through a small aperture in the splitter plate, continuing through the gas in the second channel and into the spectrometer through the shutter-valve. The gas in this channel has been processed by the incident shock only, and hence is heated to a significantly lesser degree. The operation of the splitter plate is shown in Fig. 1a, with typical radiation data given in Fig. 1b. for the series of N_2 absorption experiments performed at

Calspan.[1, 2] A test gas mixture of 10% N_2 + 90% Ne was used, giving a reflected-shock temperature of 11,300°K which provided a continuum source of radiation (I_o) over the wavelength region of interest.[8] The absorbing gas behind the incident shock was at a temperature of 6000°K.

The lower trace in Fig. 1b is from a detector monitoring the total reflected-shock radiation history at a wavelength of about 1300 Å. The upper trace is the recorded signal from one channel of the VUV spectrometer viewing radiation at 760 Å which has been partially absorbed by the incident shock-heated gas. A comparison of this signal to that obtained with the reflected-shock light source on the spectrometer side of the splitter plate gives the fraction of light transmitted through the heated gas.

This splitter-plate and spectrometer arrangement was employed for the NO absorption experiments. As discussed in previous reports[4] prior to initiating the experimental program, several computations had to be completed in order to define the experimental test conditions. Several criteria must be fulfilled in order to obtain suitable absorption data. For example, the test gas mixture, pressure and incident shock speed must be compatible with: (1) attainment of reflected shock conditions (i.e., temperature) so as to obtain a suitably heated, uniform volume of gas to serve as a continuum light source I_o, and (2) incident shock conditions of temperature and species density, so as to obtain a measurable range of absorption in the test gas.

Equilibrium shock wave computations[11] were initiated for various test gas mixtures. Based on the previous N_2 experiments, a test gas mixture consisting of 90% neon as the carrier gas, at a total pressure of 2 torr was used in the computations. Neon is used to obtain high reflected shock temperatures and is optically inactive in the wavelength range of interest, $800 < \lambda < 1100$ Å. Both incident and reflected shock conditions, over a range of shock strengths, were calculated for the following gas mixtures:

90% Neon + 10% NO
90% Neon + 10% Air (8% N_2 + 2% O_2)
90% Neon + 5% N_2 + 5% O_2
90% Neon + 2% N_2 + 8% O_2.

The calculations are described in detail in Ref. 4 and will only be briefly discussed herein. Computations were performed to determine equilibrium incident and reflected shock temperatures and NO concentration as a function of shock speed for the various gas mixtures considered. The calculations indicated that incident shock temperatures ranged from 4500-6500°K for the velocity range under consideration for the NO experiments. The corresponding reflected shock temperatures range from 8000-13,000°K.[4] The NO number density behind the incident shock was also obtained. It is this NO concentration, in combination with the wavelength-dependent absorption coefficient that determines the degree of absorption due to NO taking place in the test gas (see Fig. 1). The combined results of all these computations are used to define the shock velocity and test gas mixture used in the experiments.

Since the N_2 molecule contributes substantially to the absorption process in the wavelength region of interest, it is desirable that the N_2/NO ratio be kept to a minimum. From Fig. 2, it can be seen that the 10% air-test gas mixture yields ratios greater than 100; thus this mixture was not used in the experimental series. As the initial percentage of N_2 is decreased, the resultant N_2/NO ratio is also decreased, as can be seen from the 2% N_2 - 8% O_2 computation. Here the ratio is over an order of magnitude lower than the air results. From Fig. 2, then, it can be determined that mixtures other than air are required as the test gas.

At lower shock velocities, the reflected shock temperature is decreased, thus the resultant source radiation, I_o, is reduced substantially. At higher shock velocities, the reflected shock temperature is increased; however, the calculations showed that the absolute value of the NO concentration is substantially decreased[4] which in turn may yield very small values of absorption. The computations indicated that the absolute value of NO concentration is relatively insensitive to the initial test gas composition, differing by about a factor of 2 or 3 for the various mixtures investigated.

This can be compared to the N_2/NO ratio shown in Fig. 2, which was shown to be very sensitive to the initial test gas composition.

On the basis of these computations, the series of absorption experiments was undertaken utilizing the 2% N_2 - 8% O_2 - 90% Neon test gas mixture. For shock speeds in the range of 12,000 ft/sec, it can be seen that the N_2 concentration is about 20 times that of the NO molecule (i.e., as shown in Fig. 2). The possible absorbing species in the incident-shocked gas are then, the molecular species N_2, O_2 and NO, and the atomic species O and N. However, the NO concentration, for the shock speeds under consideration, is approximately an order of magnitude greater than that of O_2. But the absorption characteristics of the abundant atomic species must be taken into account. The presence of the N atom at these temperatures for example, leads to absorption below 850 Å, which is the absorption edge of the ground state $N \rightarrow N^+ + e$ transition. This was observed experimentally during the previous program directed at N_2 absorption coefficients.[1, 2, 3] Calculations for the present gas mixture, however, at a shock velocity of 3.8×10^5 cm/sec, indicated an absorption of only about 8% for $\lambda \leq 850$ Å due to the rather low N atom concentration. Similarly, the presence of the O atom will lead to absorption for wavelengths below 911 Å, which is the absorption edge of the ground state $O \rightarrow O^+ + e$ transition. Similar calculations indicate approximately 50% absorption for $\lambda \leq 911$ Å, due to the large number of O atoms present in the incident-shocked gas. (For these computations, the absorption cross-sections given in Ref. 12 were used). On the basis of these atomic absorption calculations, it could be seen that the molecular NO absorption measurements should be directed toward wavelengths greater than 911 Å.

For the 2% N_2 - 8% O_2 - 90% Ne gas mixture, and a nominal shock velocity of 3.8×10^5 cm/sec used in the experiments, the reflected shock temperature is 11,300° K, and the absorbing gas behind the incident shock is at a temperature of 5000°K.

II. 2. 1. 2 Experimental Program

An initial test series of shock-tube splitter-plate experiments was first undertaken. For this initial series, the explosively driven plunger which couples the VUV spectrometer to the shock tube was replaced with a LiF window adapter (see Fig. 1). Thus, wavelengths greater than about 1050 Å were observed during these tests. The primary purpose of these tests was to establish shock-tube performance and radiation characteristics of the various test gas mixtures and to compare these characteristics with measurements from a simple N_2 - Neon test gas. Figure 3 shows a schematic of the experimental arrangement employed for the experiments, showing three possible endwall configurations, and either a LiF window or explosively driven plunger coupling the spectrometer to the shock tube. The primary diagnostic for the shock radiation is the three-channel vacuum-ultraviolet spectrometer.[8, 9, 10] A small mirror inside the spectrometer arm was used to permit a photomultiplier-filter combination to view 5100 Å radiation through the same optical path. On the opposite side of the shock tube another photomultiplier-filter assembly viewed 2300 Å radiation, and a thin-film heat transfer gauge was used to display the wall temperature rise (ΔT) due to the incident and reflected shock waves.

Approximately 6 feet upstream of the reflecting endwall, several detectors were used to monitor the radiation from the hot gas behind the incident shock wave. Here, two photomultiplier-filter combinations were used to view radiation at 2500 Å and 6000 Å, and an EMR solar-blind PMT was utilized to view radiation in the 1300 Å wavelength range. In addition, a thin-film wall ΔT gauge was also displayed to aid in the determination of the incident-shock test time. All of the wavelength intervals chosen for measurements correspond to emitting transitions in the shock heated gas mixture. Spectral intensities from these transitions have previously been recorded and used to monitor the state of the shocked gases. Similarly, the sidewall heat transfer data are used to monitor shock tube operation and repeatability.

The test gas mixtures were admitted to the shock tube through a pumping/loading manifold to an initial pressure of 2 torr. Room temperature

hydrogen, at pressures from 650 - 1350 psi, was used as the driver gas. Resultant shock speeds in this test series ranged from approximately 11,500 - 15,000 ft/sec.

The first part of the test series utlizing the LiF window adapter was described in detail in previous reports.[4] However, a brief discussion of the wavelengths investigated and preliminary results are included herein since additional measurements were obtained using the explosively driven plunger adapter. For the LiF window experiments, the grating setting was adjusted such that 1110 Å, 1180 Å and 1625 Å radiation was monitored in first order, with a bandpass of ± 16 Å. However, the detector response has dropped considerably at the longest wavelength (1625 Å) and no radiation data was obtained.

Figure 4 shows typical data records obtained for three different configurations at the reflecting endwall, all for the same shock speed in the 2% N_2 / 8% O_2 + 90% Neon test gas mixture. The data records on the right of the figure show the time history of the 5100 Å radiation (as viewed from within the VUV spectrometer through the LiF window) for the three configurations. The reflected shock radiation records (for all wavelengths monitored) are typified by a rise to a plateau-like region after the arrival of the reflected shock wave, a relatively constant value (which indicates the reflected shock test-time) and finally, a sudden increase in intensity as the test-time is ended (due to the arrival of an additional shock wave from the original reflected shock-interface interaction). For this test condition, the reflected-shock test time is seen to be approximately 130 μ sec.

Also shown on these records is the output from a thin-film wall temperature gauge located near the 2300 Å viewing port (see Fig. 3). The upper and lower records show the gauge output for: (a) a sudden rise to a very short plateau region which corresponds to the passage of the incident shocked gas, and (b) the subsequent parabolic increase in temperature which is characteristic of the heat transfer due to the reflected shock gas. These data can be compared with the trace shown in the middle record, which shows only the constant-temperature plateau typical of incident-shocked gas only; this shows the passage of the incident shock along one

side of the splitter plate. The rise in temperature after a period of about 200 μ sec shows the extent of the incident-shocked slug of gas. Superimposed on this record is the 5100 Å radiation trace from the reflected pocket on the opposite side of the splitter plate. It can be seen that the reflected-shock test time (source of i_o radiation) is properly timed with the passage of the incident-shocked gas for the absorption measurements.

II.2.1.3 Splitter-Plate Results

Previous absorption measurements [1, 2, 3] for N_2 and calculations indicated that the incident-shocked gas should be transparent at the wavelengths investigated during this test series (1110 Å, 1180 Å). However, the splitter-plate data obtained for both the 2% N_2/8% O_2 and the 10% N_2 mixtures with the LiF window indicated a substantially lower signal when the reflected pocket is on the opposite side of the shock tube, i.e., $I/I_o \approx .25$. Earlier experiments [8, 9, 10] indicated that there could be substantial absorption in the boundary layer near the explosively driven plunger entrance, if sufficient care were not taken to pump away the boundary layer. To determine if this was the cause of the reduced signals, the same wavelengths were investigated early in the explosively driven plunger test series, as described below.

Following preliminary experiments to validate the sequencing of the plunger open time, the VUV spectrometer grating was adjusted to monitor the wavelength intervals noted earlier; 1110 Å, 1180 Å and 812 Å. The third wavelength region was viewed in second order, (i.e., 1625 Å first order, 812 Å second order) since the LiF window which had previously restricted the measurements to wavelengths > 1050 Å had been removed. In this windowless coupled configuration, the preliminary measurements indicated the following for the 2% N_2/8% O_2/90% Neon gas mixture at a shock speed of 3.8×10^5 cm/sec:

wavelength	1110 Å	1180 Å	812 Å
I/I_o experiment	~ 0.94	~ 0.94	~ 0.22
I/I_o calculated	0.95 (N_2 only)	1.0 (N_2 only)	0.35 (O + N only)

At the wavelengths of 1110 Å and 1180 Å, these later experiments indicated that the gas is essentially transparent, as opposed to the I/I_o value of ≈ 0.25 obtained when the LiF window adapter was used. These results are in substantial agreement with measurements obtained earlier [8, 9, 10] which indicated that there could be a substantial effect of the boundary layer on the measurements if sufficient care were not taken to pump it away.

Also indicated in the table are approximate calculated values of I/I_o. At wavelengths of 1110 Å and 1180 Å, the calculations assumed that only N_2 was responsible for absorption; the experiments are in substantial agreement with the calculations indicating that the presence of NO had no effect on the measurements. At 812 Å, the calculations were performed with O and N atoms as the principal absorbing species. At this wavelength the experimental value was smaller indicating that the NO molecule may be contributing to the absorption process.

Additional experiments were performed at various VUV spectrometer grating settings as follows for the same mixture and shock speed:

wavelength	895 Å	970 Å	706 Å
I/I_o experiment	~ 0.13	~ 0.22	~ 0.30
I/I_o calculated	0.20 (N_2 + O alone)	0.535 (N_2 alone)	0.25 (O + N alone)

Again, the calculations at each wavelength were performed for the dominant absorbing species (other than NO) as indicated. At 895 Å and 970 Å, the experimental values are considerably smaller than the calculated values, again indicating that the NO molecule may be contributing to the absorption process.

These results are shown in Figure 5, which presents the ratio I/I_o as a function of wavelength for both the experimental and calculated values. Shown for the calculations are the contributions for each specie as indicated, and the overall computed absorption for the incident-shocked gas mixture, excluding the presence of NO. As noted earlier, the presence of O atoms must be taken into account for wavelengths below 911 Å, and below 850 Å, the N atoms contribute approximately 8% to the absorption process. The experimental data can be compared with the computed values,

and any substantial deviation may be attributed in part to absorption from the NO molecules present in the shocked gas.

For wavelengths greater than about 1100 Å, the gas is essentially transparent, with no substantial absorption from either N_2 or NO. Also, at the shortest wavelength investigated to date, 706 Å, there appears to be no substantial NO absorption and the O and N contributions can essentially account for the measured data. However, at wavelengths of 812 Å, 895 Å, and 970 Å, the experimental results are substantially below the calculations, and NO abosrption may play a major role in this wavelength region.

At 895 Å, for example, if the difference berween the calculated and measured values of I/I_o were attributed only to vibrationally excited NO, an absorption coefficient of $k_{NO} \approx 9,900\ cm^{-1}$ is obtained. This can be favorably compared with a measured value in cold NO of [5,6] approximately $9000\ cm^{-1}$ at 898 Å. However, at the 812 Å and 970 Å wavelengths, if the indicated difference were ascribed only to NO, the absorption coefficients obtained are too high: at 812 Å, $k_{NO} \approx 13,000\ cm^{-1}$ and at 970 Å, $k_{NO} \approx 24,000\ cm^{-1}$. Although there is a peak in the cold NO absorption coefficient near 810 Å, i.e., $k_{NO} \approx 3000\ cm^{-1}$, the experimentally determined value is much greater than this.

The tabulations given in Ref. 12 indicate several strong lines of the O atom particularly in the 970 Å bandpass, and to a lesser extent, in the 812 Å bandpass. The 895 Å bandpass is relatively free of strong lines, and the additional absorption observed may in fact, be attributed to the NO molecule. The experimental data at 812 Å and 970 Å, however, may be compromised due to the presence of strong lines. Thus, attributing the additional absorption at these wavelengths only to the NO molecule would lead to extremely large absorption coefficients, as indicated previously.

II.2.1.4 Sidewall Measurements

In addition to the splitter-plate measurements discussed previously, additional measurements of the nonequilibrium radiation overshoot behind the incident shock were also obtained during the test series, utilizing the instrumentation indicated in Fig. 3. This sidewall data was obtained prior to the installation of the highly spatially resolved VUV and UV diagnostics discussed later in this report. Typical data for several of the test gas

mixtures is shown in Fig. 6 for different gas mixtures and shock speeds. In general, the radiation data shown is typified by a sudden increase upon passage of the incident shock past the viewing port. The radiation then reaches an overshoot maximum close to the shock front and subsequently decays toward the final equilibrium value.

The measurements show substantial radiation at 6600 Å for only the 10% N_2 test mixture, (Fig. 6a); this radiation arises from the N_2 (1+) band system. Differences in the radiation time history for the 1300 Å wavelength are readily observed for the different test gas mixtures shown in the figure. For 10% N_2, there is a well defined overshoot occurring about 50 μ sec after shock passage (Fig. 6a). However, for the 10% NO mixture (Fig. 6b), the data indicate a long plateau-like region, with no clearly definable nonequilibrium overshoot. This is similar to the results obtained for the 2% N_2/8% O_2 gas mixture (Fig. 6a).

For all the gas mixtures, the 2500 Å, measurements showed a clearly defined overshoot maximum occurring near the shock front. The data are shown at two different oscilloscope sweep speeds, the larger record having expanded the time near the shock front. For the 10% N_2 mixture, this radiation, which arises from the N_2 (4+) band system, does not show the rapid decay apparent in the other records, but rather, a slow decline toward the equilibrium level. When NO is present behind the shock wave, the peak overshoot value at this wavelength increases substantially. This can be seen in Fig. 6a when comparing the 2500 Å data for the same nominal shock velocity. For the 2% N_2/8% O_2 test gas, NO is formed behind the shock wave. The peak radiation value is approximately 10 times greater for the N_2/O_2 mixture than for the pure nitrogen case. The radiation at this wavelength is dominated by the NO (γ) system when the NO molecule is present. This is also shown in Fig. 6b for a slower shock velocity. When NO is present initially in the test mixture (i.e., the 10% NO gas) the peak value is approximately 8 times the value of that measured when NO is formed from the initial N_2/O_2 species.

The lower data record in Fig. 6b, with a time sweep of 20 μ sec/div, shows the complete 2500 Å time history for the duration of the incident-shocked

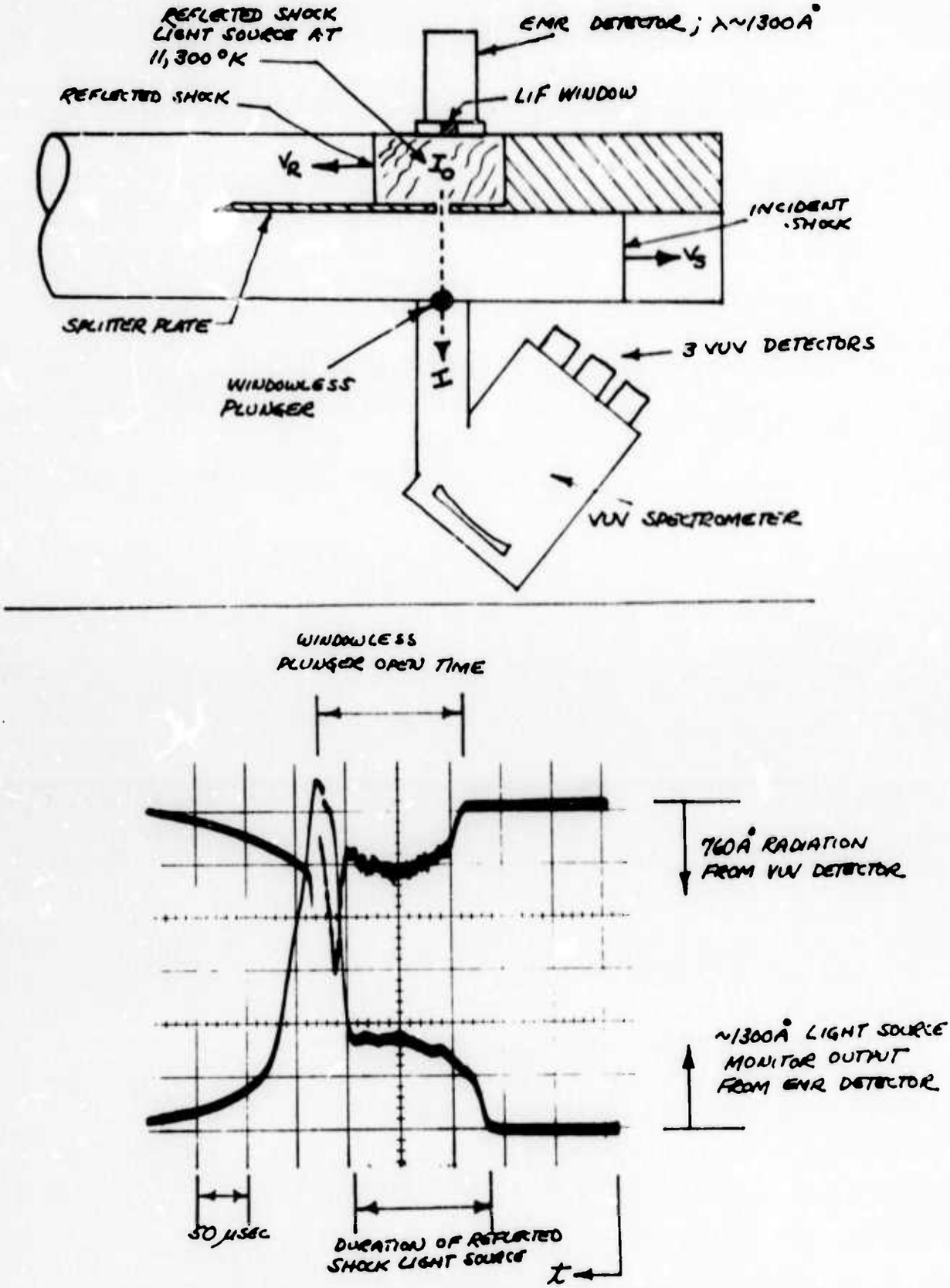

Figure 1. SPLITTER-PLATE EXPERIMENTAL CONFIGURATION

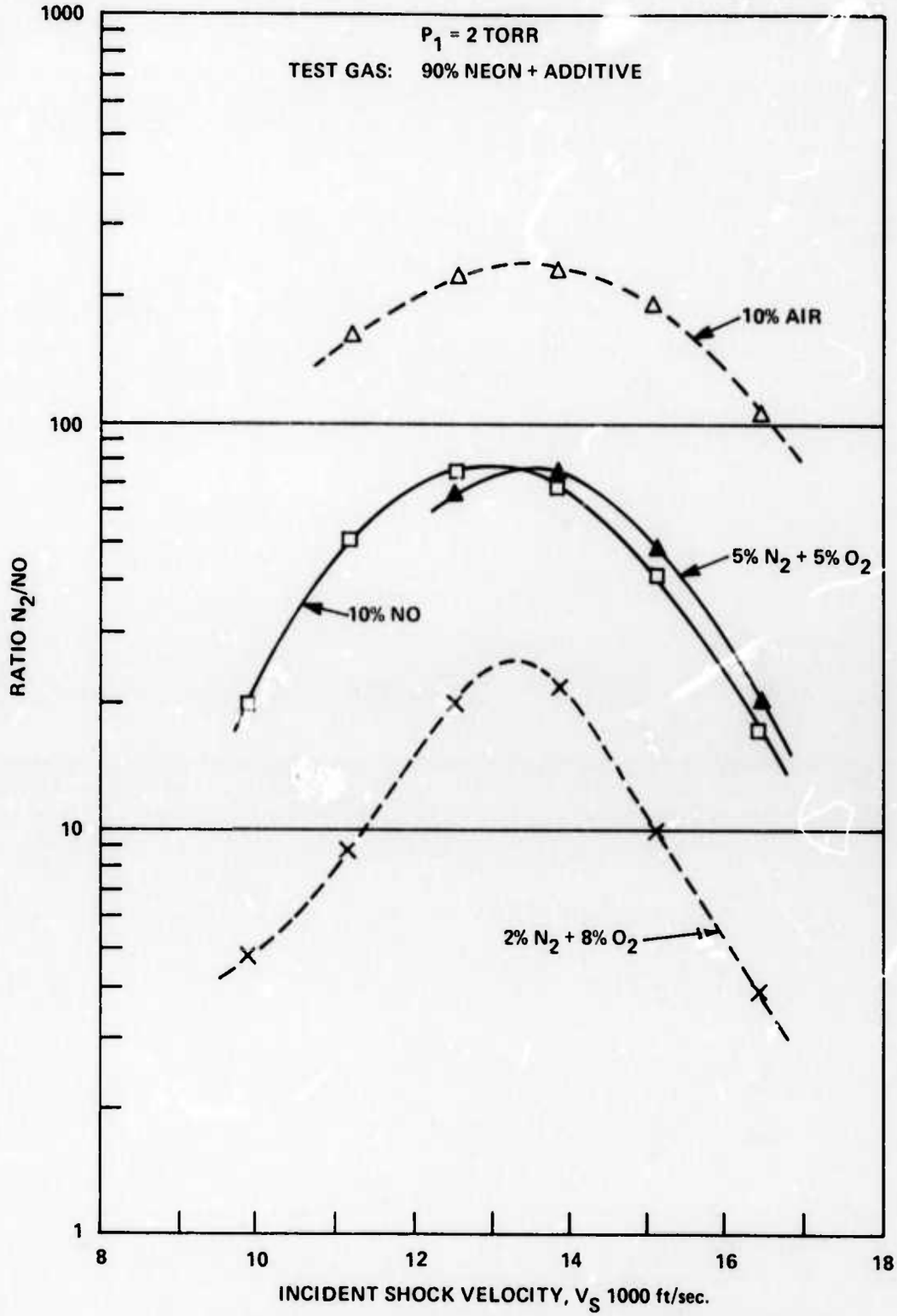

Figure 2 CALCULATED RATIO OF N_2/NO CONCENTRATION BEHIND INCIDENT SHOCK WAVE

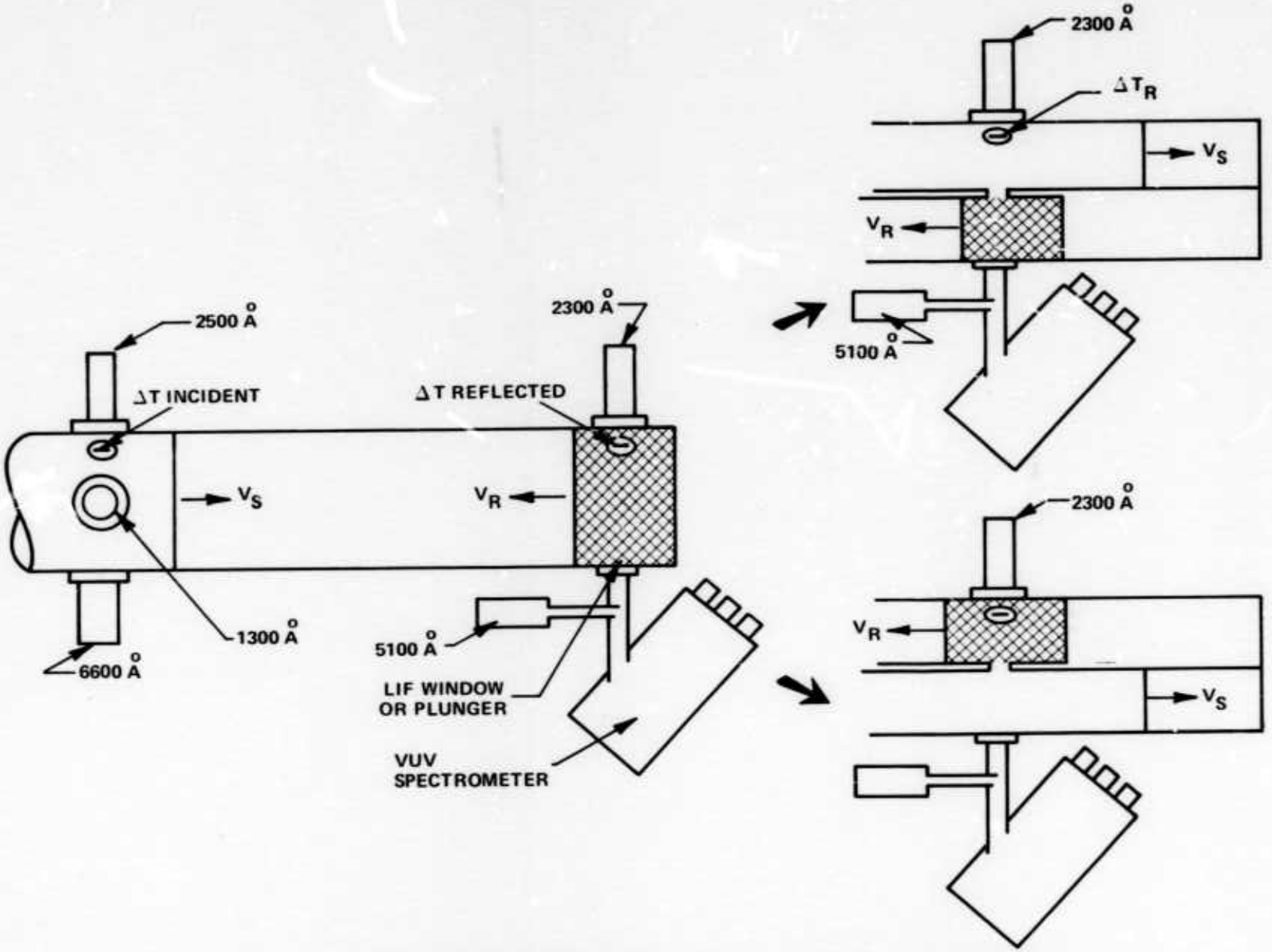

Figure 3 SCHEMATIC OF EXPERIMENTAL SHOCK-TUBE CONFIGURATIONS

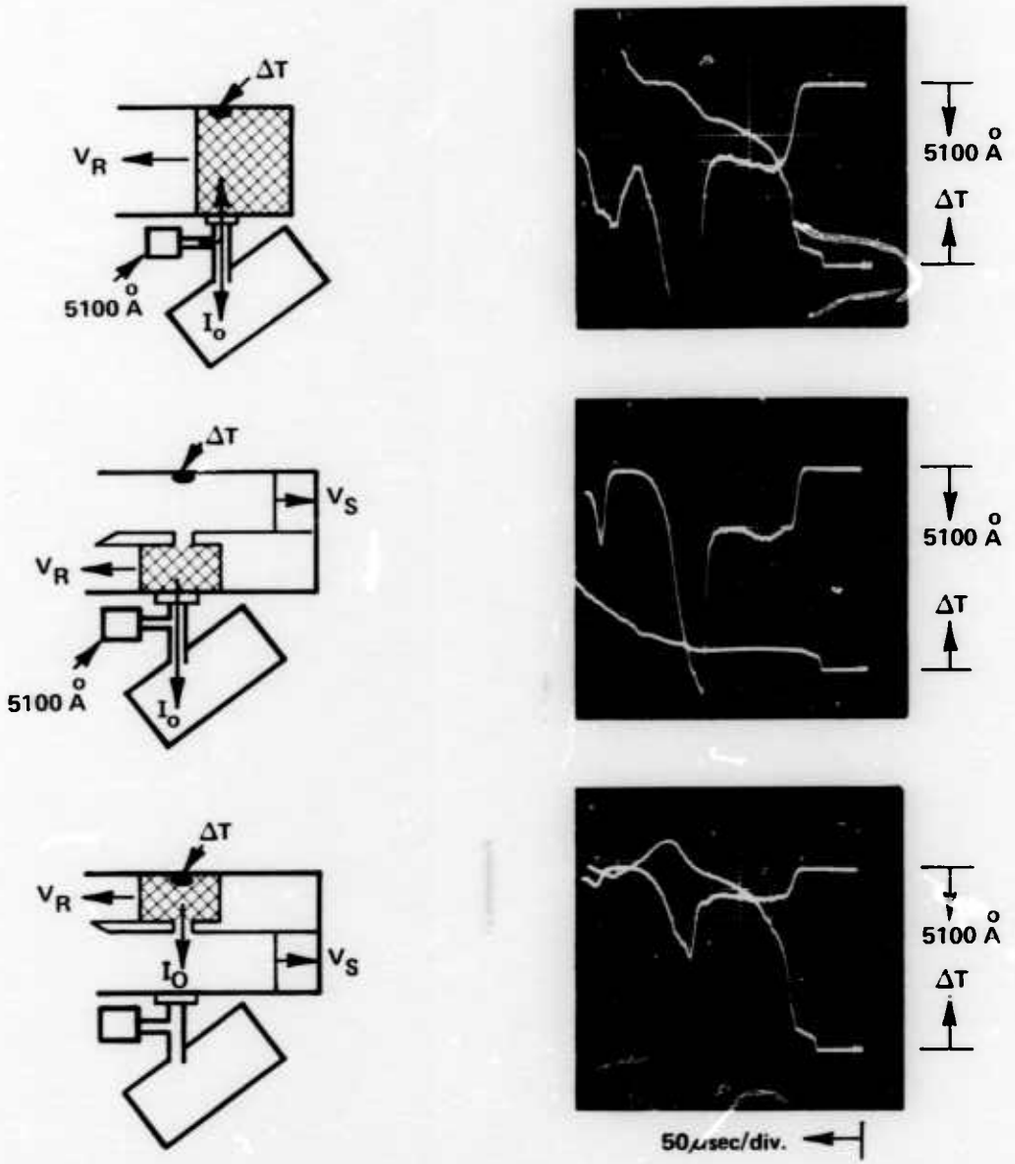

Figure 4 REFLECTED SHOCK MEASUREMENTS: 2% N_2/8% O_2 + 90% Ne
P_1 = 2 TORR, V_S = 12,500 ft/sec., $T_R \approx 11{,}300\ ^oK$

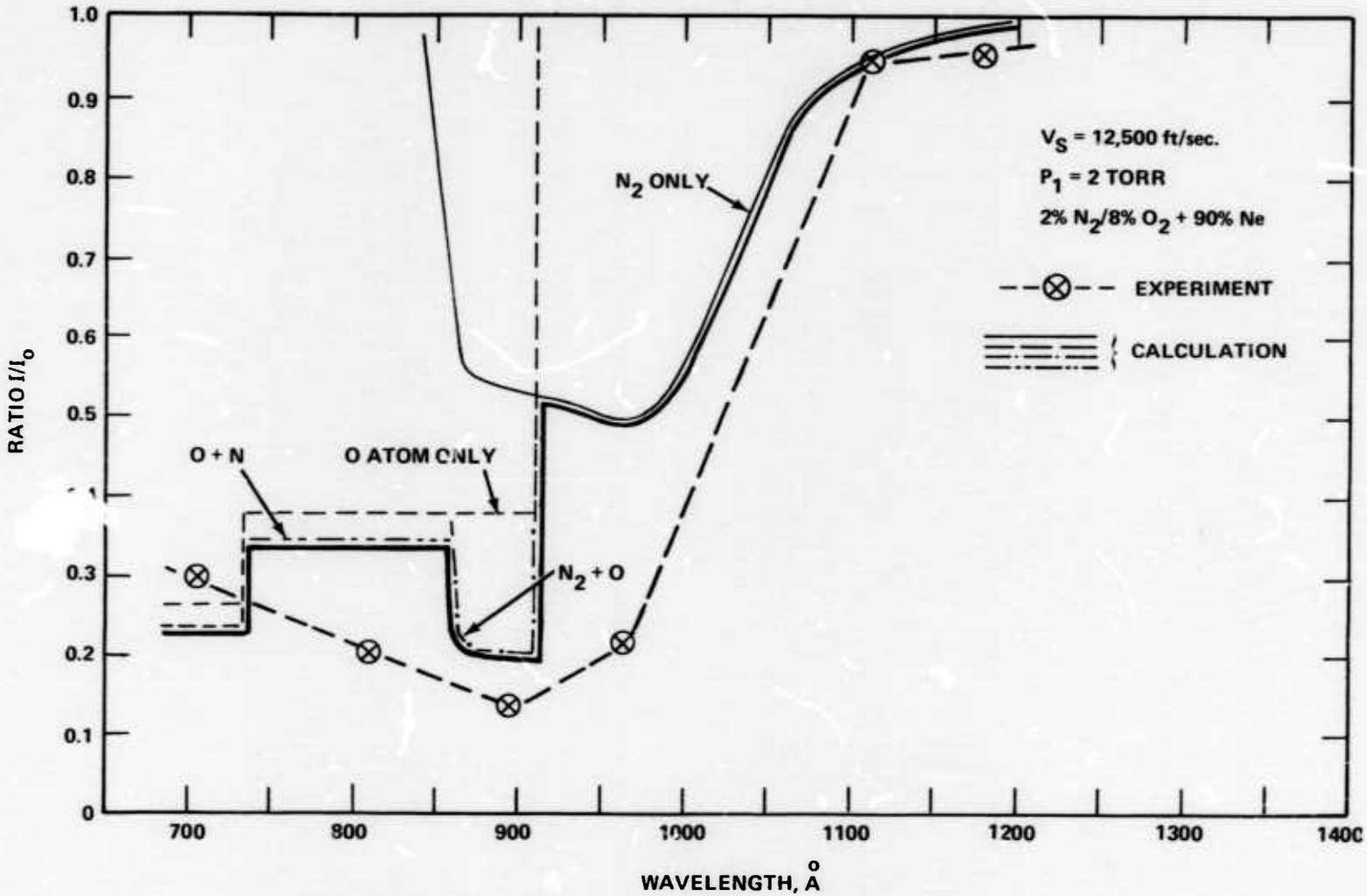

Figure 5 ABSORPTION AS A FUNCTION OF WAVELENGTH; INCIDENT SHOCK TEMPERATURE ~5,000 °K

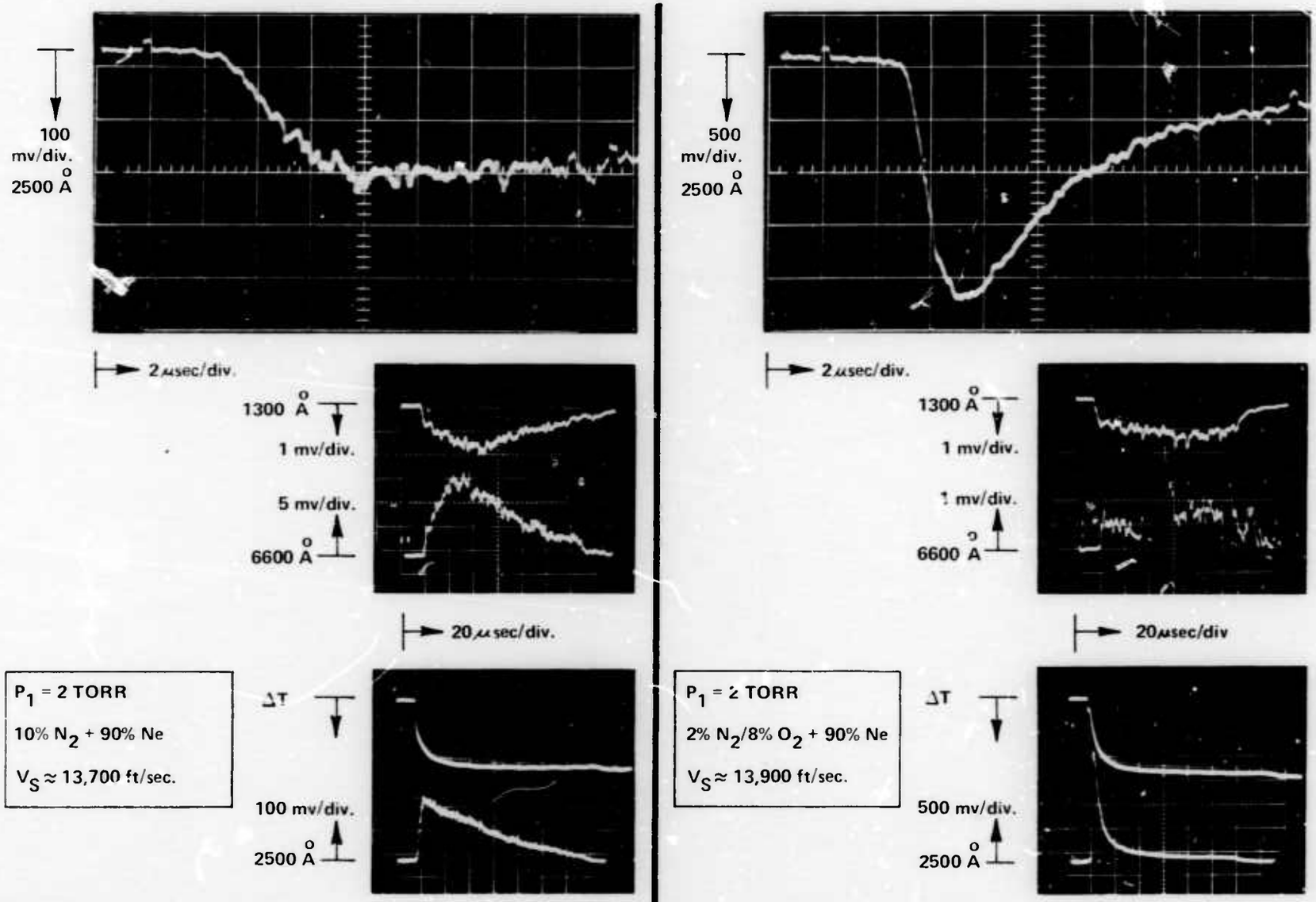

Figure 6a TYPICAL INCIDENT SHOCK DATA

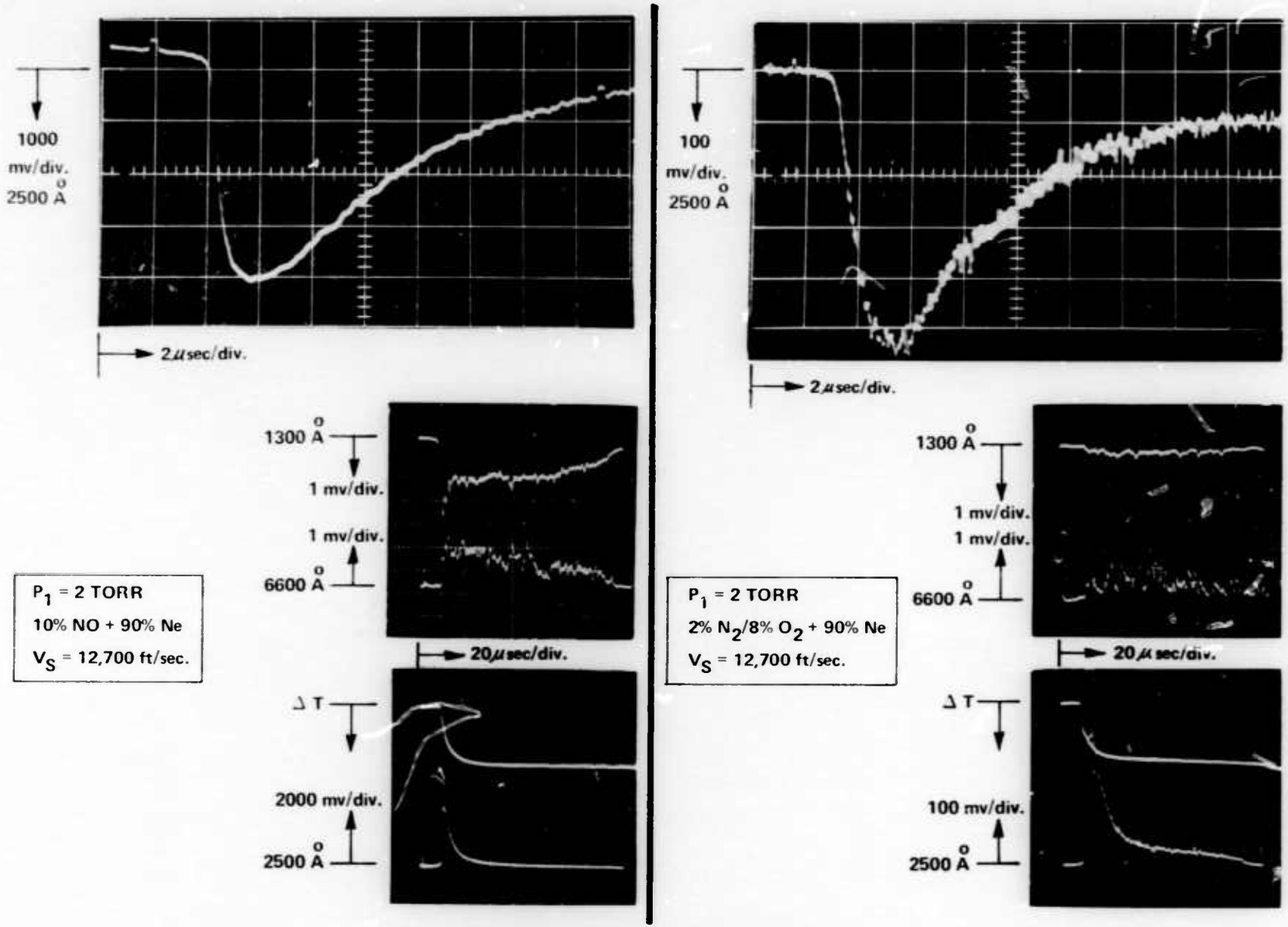

Figure 6b TYPICAL INCIDENT SHOCK DATA

test gas. It can be seen that this nonequilibrium overshoot occurs extremely early in the approximately 160 μ sec of test time. This record can be compared to the sidewall ΔT record which also shows the duration of the test gas slug; the increase in ΔT near the end of the record indicates the end of the incident shock test time at this station in the shock tube. By comparing this record with the middle record shown in Fig. 4, it can be seen that the splitter-plate VUV absorption measurements are obtained when the incident-shocked gas has substantially obtained its final equilibrium level.

II. 2. 2 Sidewall Radiation Overshoot Measurements

II. 2. 2. 1 Experiment Definition

At high altitudes, the low densities and correspondingly decreased collision frequencies in the shocked gas produce an appreciable lag in the kinetics which determine species concentrations and energy partition in the internal modes of the molecules. For typical reentry gas cap temperature, the electronic excitation rates for the radiating states dominate the calculation of the nonequilibrium ionizing radiation flux from the bow shock. The aims of the emission experiments described in this section were to verify previous data [1, 2, 3] necessary for the postulation of excitation mechanisms for high lying energy states of N_2. The experiments were designed to determine the radiation overshoots behind strong shock waves for the states of N_2 pertinent to the VUV photoionization problem.

Excitation of the high-lying states are critical to the present problem, but it was decided to make simultaneous measurements of several other triplet states. These states give rise to band systems in more accessible regions of the spectrum, and for this reason have been measured and used as diagnostics in many shock tube studies; see following schematic of the relevant energy levels for nitrogen studied in this experimental series:

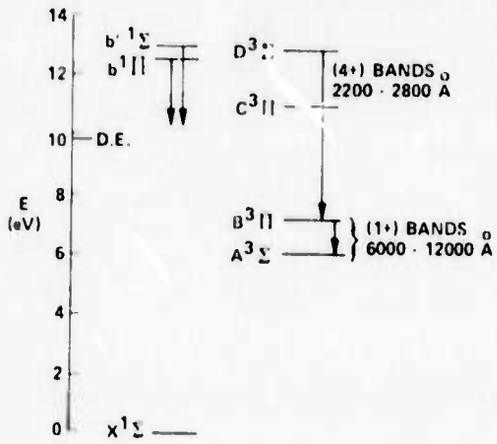

The $b'\ ^1\Sigma$ and $b\ ^1\Pi$ states are the most likely candidates for the source of VUV radiation in the region 800-1800 Å. Of additional interest is the state, which lies at 12.8 ev, well into the energy region of interest, giving rise to the (4+) band system. Thus, as an aid to the interpretation of excitation data, simultaneous measurements were made on the $D\ ^3\Sigma$ (4+), $B\ ^3\Pi$ (1+), and the combined $b'\ ^1\Sigma$, $b\ ^1\Pi$ VUV band systems. Interference filters with 200 Å bandpasses were used at 2500 Å and 6600 Å respectively for the 4(+) and (1+) measurements. A detailed discussion of the sidewall optical systems will be given in Section II.2.2.2.

A series of experiments was completed, in which shock waves at velocities from 14,000-17,000 ft/sec were driven into nitrogen at an initial pressure of 1/2 torr. This corresponded to hydrogen driver pressures ranging from 675-4,000 psia. Figure 7 indicates the shock tube performance under these conditions; the experimental shock velocity data was obtained from the thin film gauges and is representative of the velocity (V_s) approximately 6 feet from the endwall (i.e. 24 feet from the diaphragm). The theoretical curve [13] is for idealized H_2 driving N_2, and a nitrogen sound speed of 1158 ft/sec was used. The observed velocities are less than predicted at the lower shock strengths, but are seen to approach the theoretical curve at higher shock speeds. Typical shock velocity histories are presented in Figure 8 showing shock attenuation over the last 6 feet of travel in the tube. The location of the sidewall optics is near station #4, approximately 6 feet from the shock tube endwall.

II.2.2.2 Experimental Program

Optical requirements for high spatial resolution in making radiation overshoot measurements are very rigid. The nonequilibrium overshoot occurs within a few microseconds of the shock arrival and this time-to-peak may be on the order of one microsecond. A somewhat more detailed discussion of this subject is given in Ref. 1. This requirement is met by employing an optical system that uses slit images rather than physical slits at the shock tube. A spherical mirror images the two slits, one at the window of the shock tube and the other at the far wall of the shock tube. These two

aperture images define the volume of the shock tube from which gas radiance is measured. Further, the use of slit images to define the field of view precludes scattered stray light usually obtained from the edges of physical slits near shock tube windows.[15] The slit dimensions, which are on the order of 1 mm by 3 mm, define an extremely narrow field of view giving rise to a sharply defined radiation profile as the shock wave passes. This arrangement is illustrated schematically in Fig. 9. On one of these optical units, a phototube (EMI No. 9526B) was mounted with an OTI No. 250 filter that observes radiation in the wavelength region around 2500 Å. On the matching optical unit across the tube an EMR No. 641J photomultiplier tube was mounted viewing VUV radiation in the wavelength region between 1050 Å (determined by the lithium fluoride cutoff wavelength) to approximately 1800 Å. The spectral response characteristics of this photomultiplier tube are indicated in the following figure:

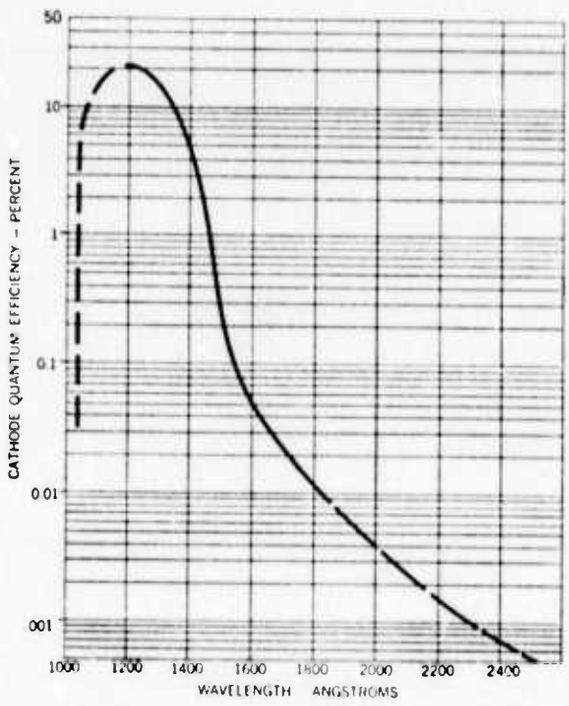

TYPICAL
SPECTRAL RESPONSE
CHARACTERISTICS

Both sidewall systems are connected to vacuum and helium purge lines. The VUV photomultiplier system was purged with helium and evacuated three times prior to each shock tube test. During the experiment it was left at positive helium pressure to avoid strong O_2 absorption characteristic of the VUV wavelength region. Although the unit viewing 2500 Å has the same pump-purge capability, it was not necessary for these measurements so this unit was left at ambient conditions for each run. Alignment of the two systems was checked by removing both the EMI and EMR photomultiplier tubes, and illuminating one set of slits with a light source. Adjusting screws at both the spherical mirror and plane mirror locations allow for corrections.

A third optical system was used to view the incident shock radiation overshoot in the red at approximately 6600 Å. This system, which is shown in the inset at the upper right of Fig. 9, also employs the double slit technique to establish a narrow field of view across the tube. An adapter flange with a sapphire window couples the system to the shock tube.

II.2.2.3 Sidewall Results

All three incident optical systems are located a few inches downstream of the thin-film gauge located at station four, which triggers the scopes recording the three photomultiplier signals. Typical data records are shown in Fig. 10 for a 15,3000 ft/sec shock into 1/2 torr of nitrogen. The short distance from station four to the location of the incident optics is enough to provide a baseline (zero signal condition) before a signal is observed as the shock enters the field of view of the optical systems. The red and VUV incident signals rise sharply, having a time-to-peak on the order of 2 μ sec. The signal tails off in approximately 35 to 40 μ sec. The 2500 Å radiation trace has a slower more pronounced rise with a time to peak on the order of 6 μ sec. The peak signal, as well as the time-to-peak, for all three incident systems was recorded as a function of velocity for each of the run conditions. Figure 11 shows the variation of the peak overshoot intensity as a function of shock strength. The data is normalized by the actual detector output for each system obtained at the lowest shock velocity (i.e. 14,000 ft/sec). Thus, the related signal strength variation with shock velocity can be observed

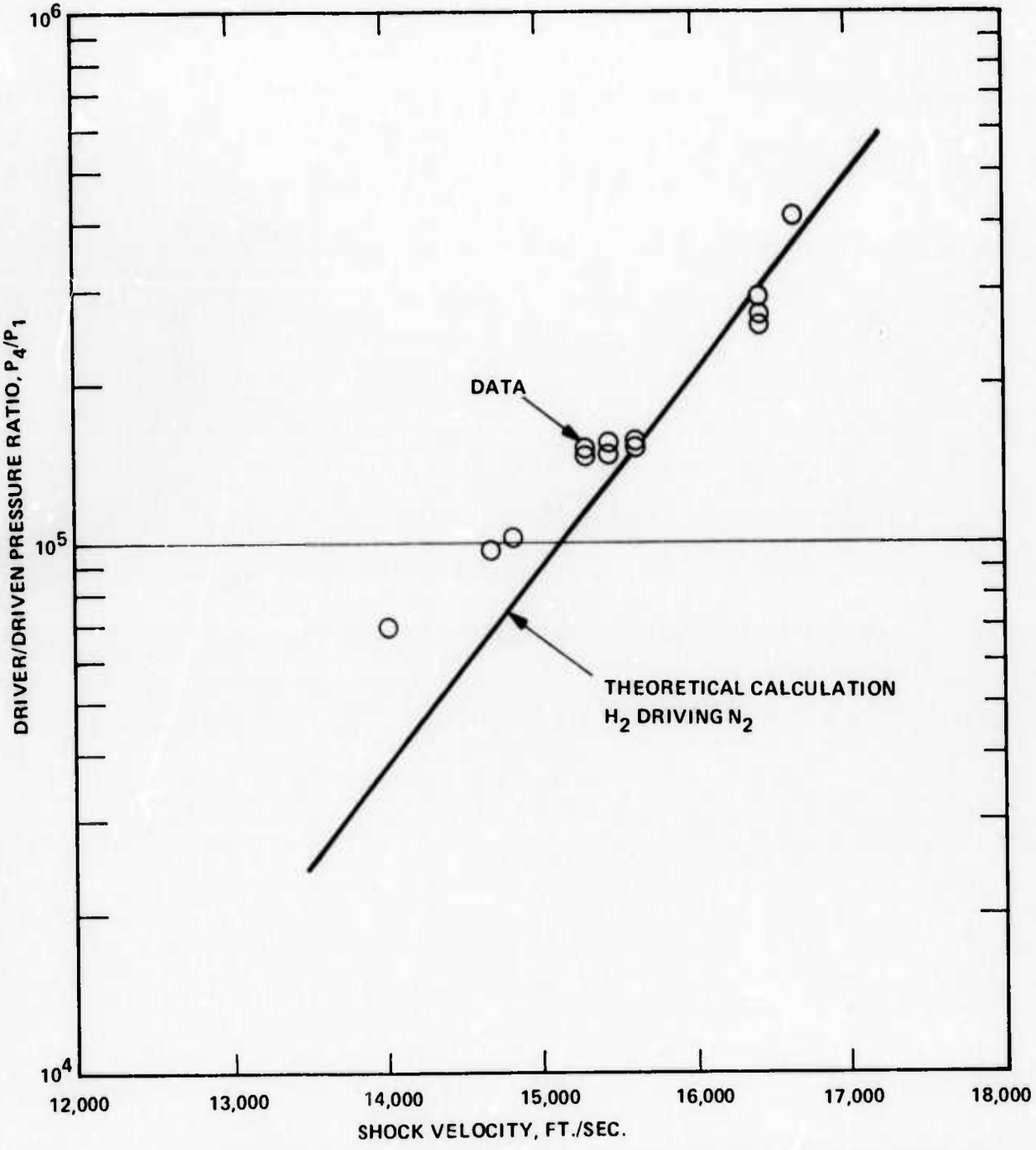

Figure 7 SHOCK TUBE PERFORMANCE DATA (SHOCK VELOCITY MEASUREMENTS AT INTERVAL C, SEE FIGURE 8)

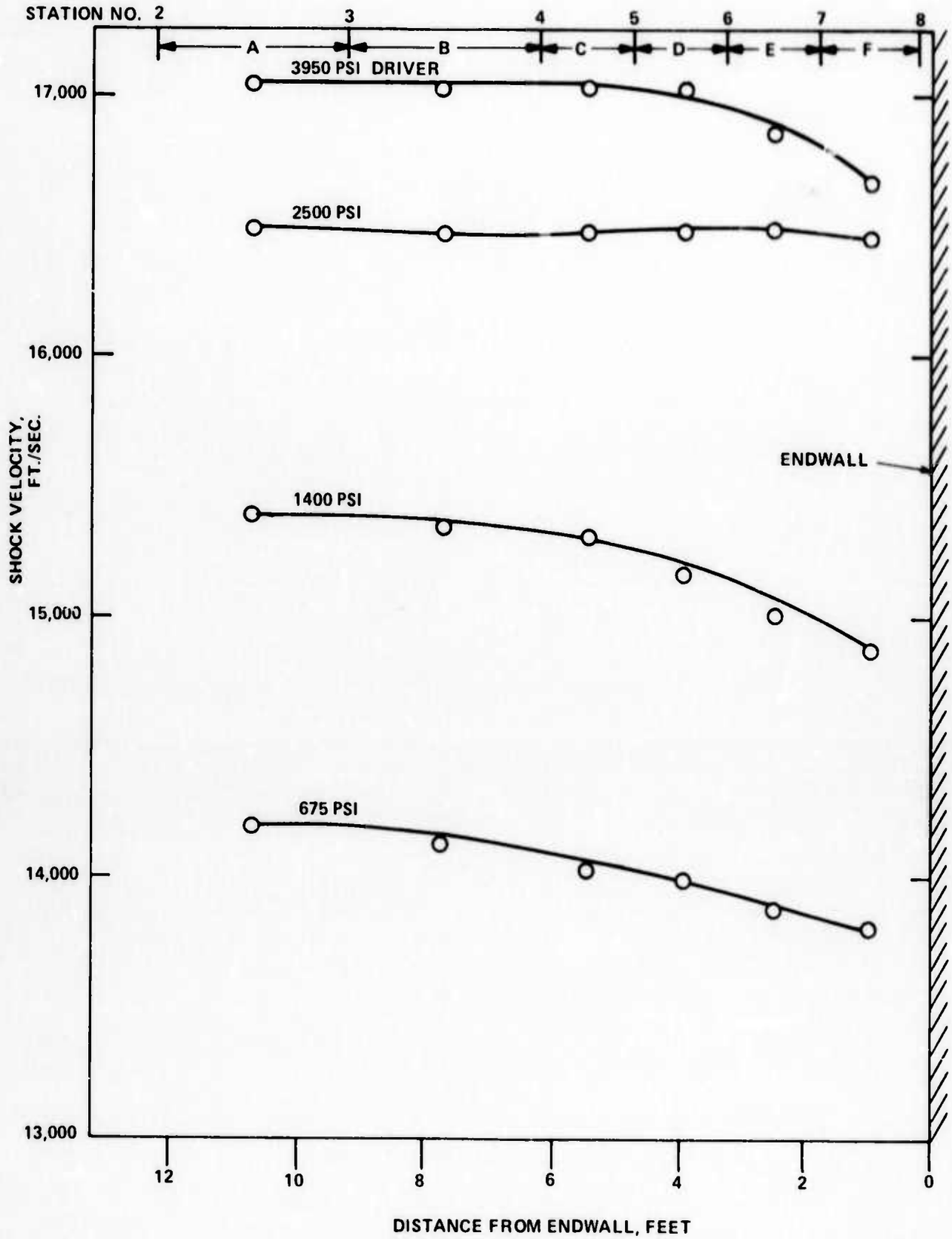

Figure 8 INCIDENT SHOCK VELOCITY; P_1 = ½ TORR NITROGEN, HYDROGEN DRIVER

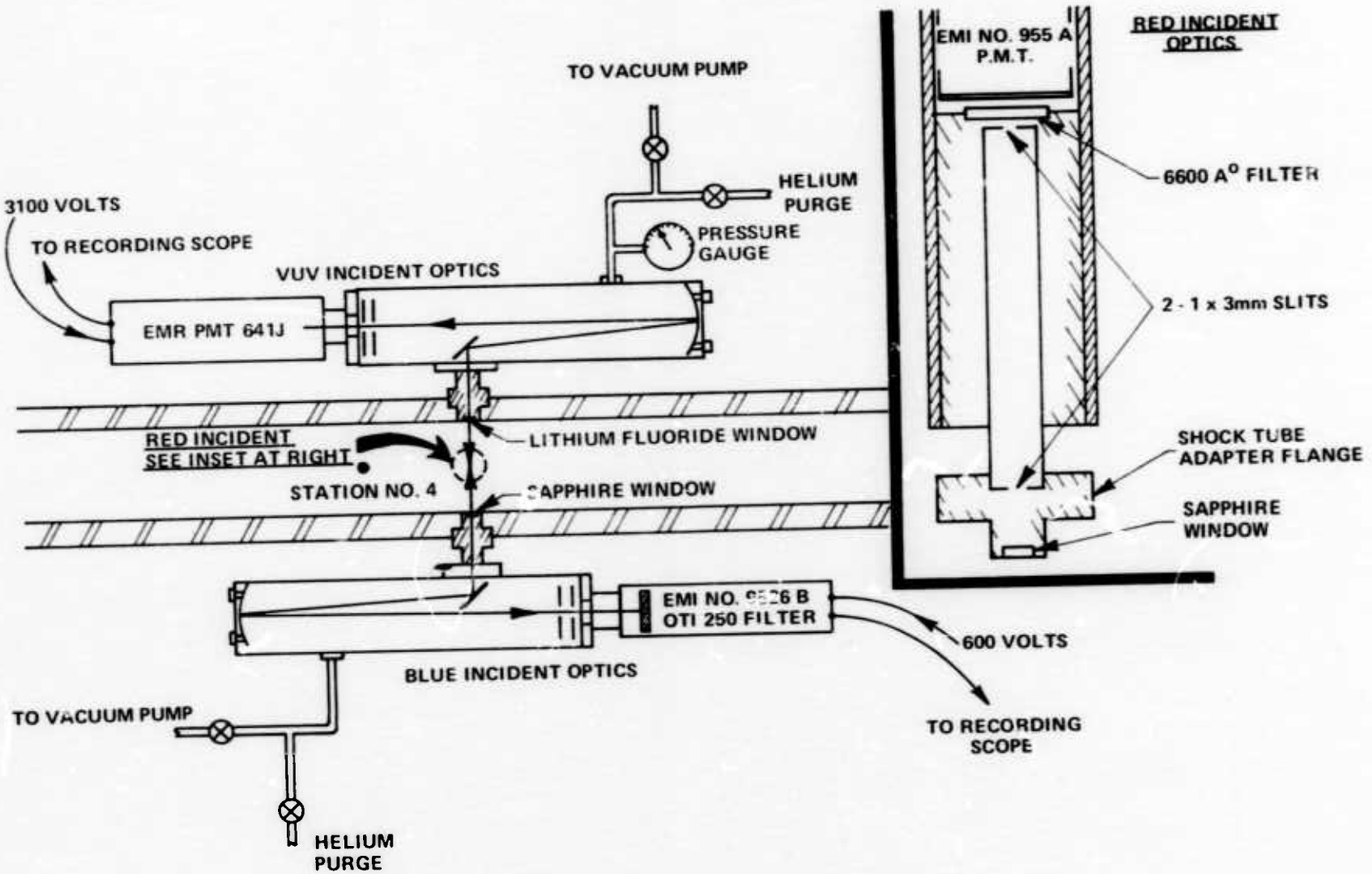

Figure 9 SCHEMATIC OF INCIDENT OPTICS CONFIGURATION

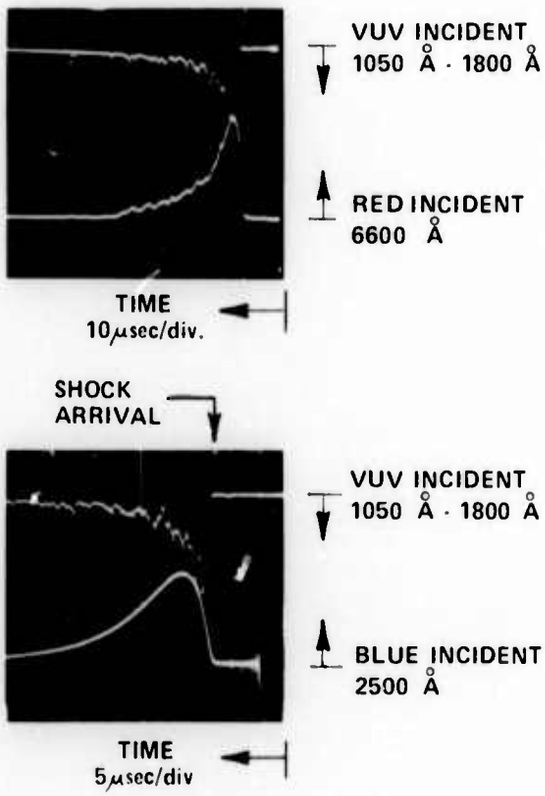

Figure 10 INCIDENT SHOCK RADIATION DATA SHOWING NONEQUILIBRIUM OVERSHOOT
$V_S \approx 15{,}300$ ft/sec; $P_1 = \frac{1}{2}$ TORR NITROGEN

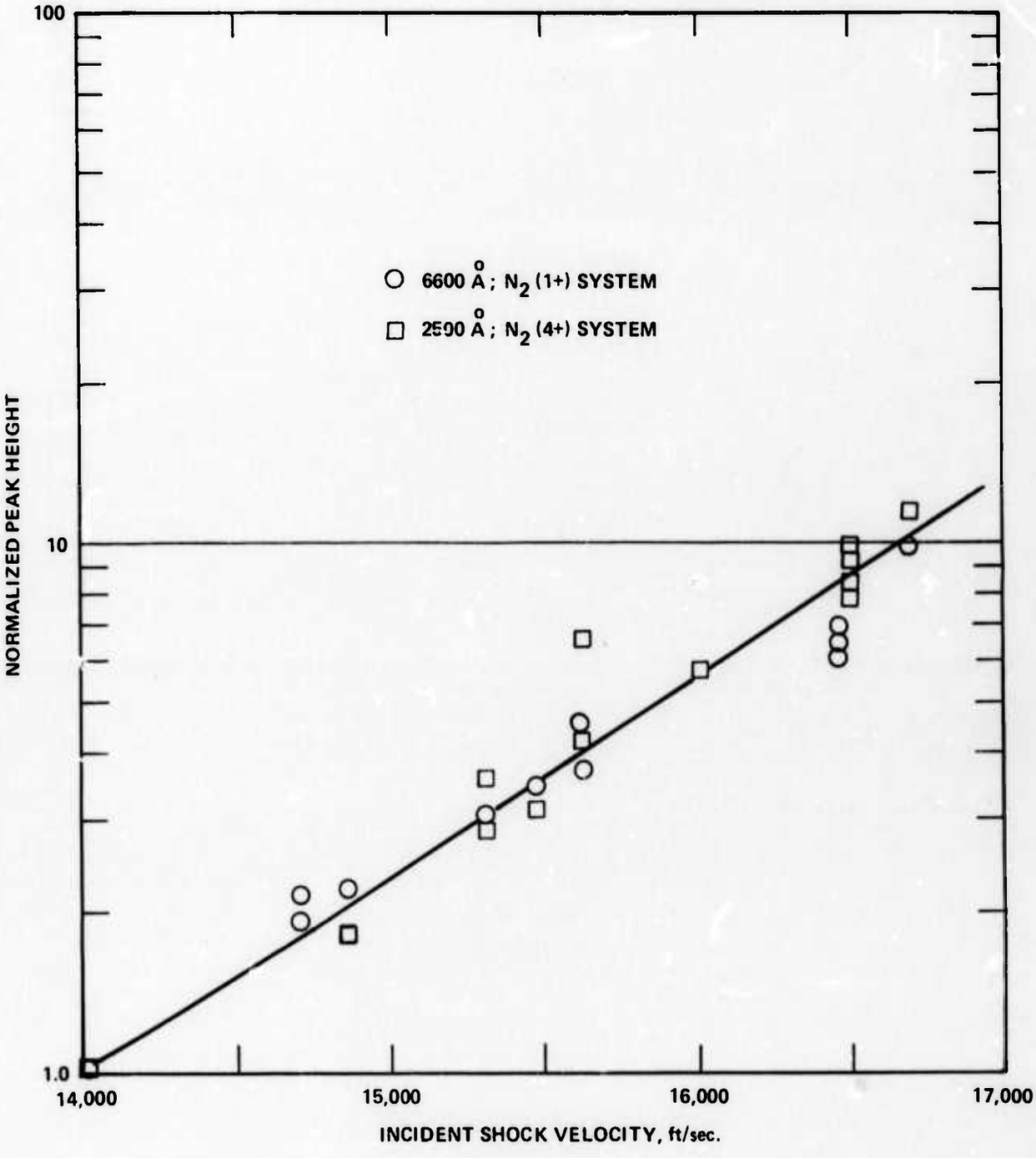

Figure 11 NORMALIZED PEAK OVERSHOOT RADIATION; P_1 = ½ TORR NITROGEN

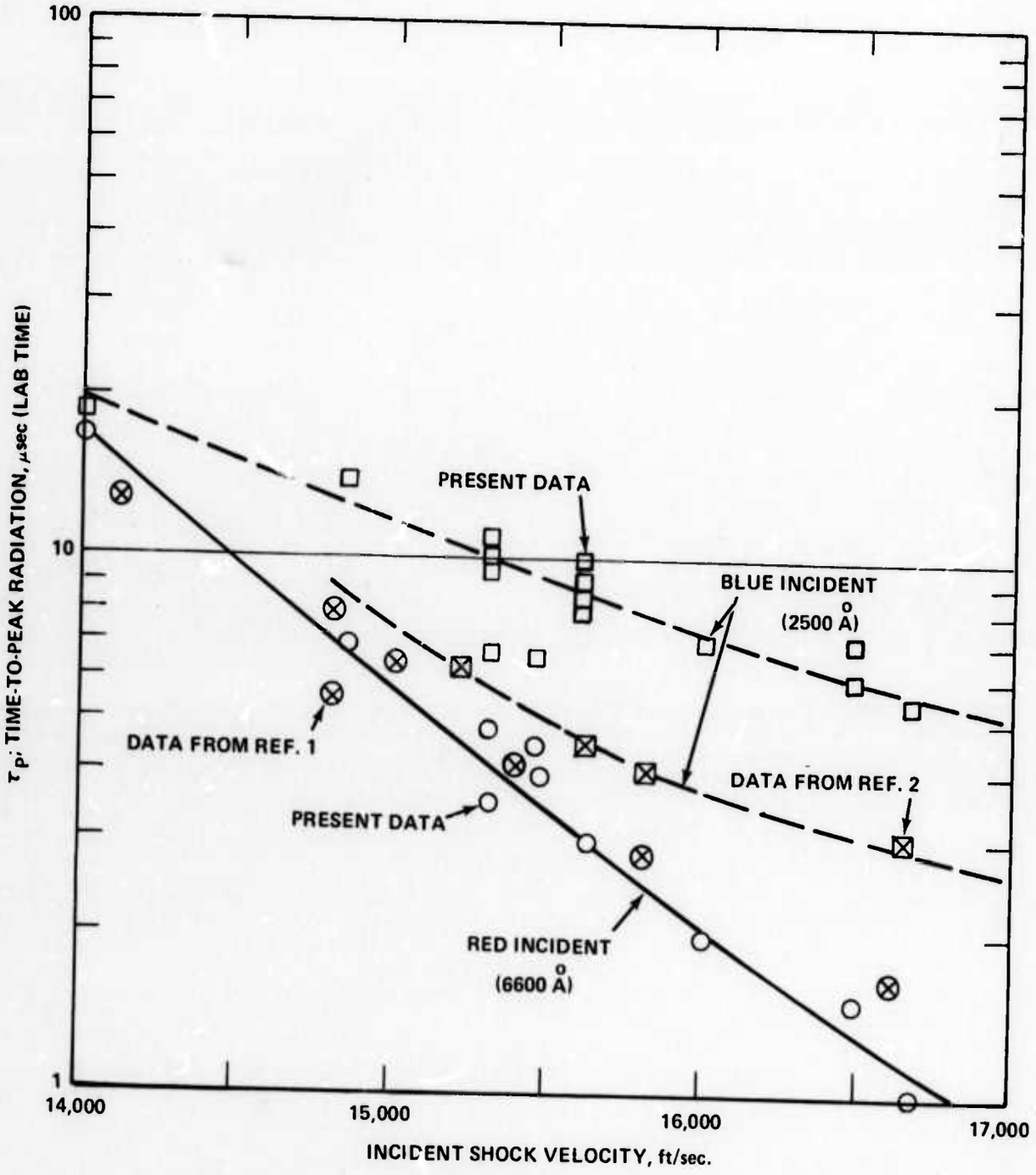

Figure 12 TIME-TO-PEAK RADIATION BEHIND INCIDENT SHOCK WAVE; P_1 = ½ TORR NITROGEN

for the radiating systems. Both the blue (2500 Å) and red (6600 Å) overshoot peak heights are seen to vary by a factor of ten over the shock velocity range investigated in the program. This variation is in agreement with earlier measurements [1, 2] which also indicated a factor of 10 increase in overshoot intensity in both systems for the same velocity range. During this present experiment VUV overshoot data was not obtained for every test, however, previous measurements [1, 2] with a less refined optical system showed a variation in overshoot peak height for the VUV of approximately a factor of 20-25 for the same velocity range. Thus, a greater dependency on shock strength (i.e. post-shock temperature) is observed for the radiating system arising from direct excitation to extremely high-lying levels in nitrogen.

Figure 12 presents results for the time-to-peak radiation measurement in the laboratory coordinate system, see Fig. 10. The present data for the red system (N_2 1+) are in close agreement with previous measurements, [1] at Calspan and elsewhere, see Refs. 13 and 14. The time-to-peak measurements for the (4+) system obtained in the present experiments appear to be about a factor of two greater than the preliminary data reported in Ref. 2. That preliminary data was obtained prior to the installation of the upgraded optical systems shown in Fig. 9, which should yield reliable spatially resolved measurements. The indication from the data is that the N_2(1+) system is excited considerably faster than the (4+) system at the shock velocities investigated during the experimental series. It should be noted that previous measurements [1] of the time-to-peak radiation for the VUV system, showed an extremely short excitation time for the high-lying b and b' states. VUV time-to-peak values of approximately 1/2 of the red data shown on Fig. 12 were obtained throughout the velocity range.

II. 2. 3 Endwall Radiation Measurements

II. 2. 3. 1 Experiment Definition

The VUV radiative flux emerging from the shock front ahead of a re-entering vehicle has been calculated[1] utilizing an excitation model developed based on the experimental measurements of nonequilibrium overshoot and time-to-peak values obtained from previous measurements and

verified during the present program, see Section II. 2. 2. A substantial portion of the present experimental program was spent in developing shock-tube endwall diagnostic systems to view axially up the shock-tube and obtain measurements of the radiation from advancing shock fronts. These endwall measurements would serve as an additional data base with which to verify the numerical predictions discussed in Ref. 1. Measurements were obtained for both the red (N_2 1+) and VUV systems of nitrogen at shock velocities ranging from 14,000-17,000 ft/sec.

II. 2. 3. 2 Experimental Program and Results

This section of the report presents a description of the experimental configurations and components employed to obtain the VUV and red endwall measurements, viewing axially up the shock tube to observe the oncoming shock front. Optical measurements obtained from this configuration may be compromised due to absorption from the low-pressure test gas in the intervening region between the endwall and the oncoming shock front. The experimental configurations are designed to obtain radiation from the shock front during the last 6 feet of travel, i. e. from the sidewall optical systems to the endwall. For the VUV wavelength region, room-temperature nitrogen absorption data is available, such as shown in Figure 13.[6] The structured absorption indicates absorption coefficients (k) ranging from 1-1000 cm^{-1}, with lowest values in the wavelength region near 935 Å and 955 Å. Thus, spectrally resolved measurements in these wavelength intervals would be least affected by absorption in the intervening test gas.

An approximate calculation was performed to indicate possible absorption effects due to nitrogen, as a function of distance upstream from the endwall, for several absorption coefficients. The calculation was performed for 1/2 torr of nitrogen as the intervening test gas, and covers the last 6 feet of travel in the tube. The results are shown in Fig. 14. For absorption coefficients greater than 10 cm^{-1}, absorption may be substantial for path lengths much greater than 4 feet.

One of the experimental configurations employed for this part of the program is shown schematically in Fig. 15. Two other endwall systems

that were also employed are not illustrated in this schematic, but will be discussed later in this section. The VUV spectrometer utilized for the splitter-plate measurements (see Section II.2.1) was reconfigured to obtain endwall radiation measurements by viewing axially up the shock tube at the oncoming shock through a 2 mm port centered on a flange adapter that connects the spectrometer to the shock tube. The spectrometer in this configuration is thus illustrated schematically in Fig. 15. The adapter flange was fabricated so that the spectrometer would be coupled to the shock tube endwall in a windowless manner. The flange houses the explosively-driven plunger apparatus and allows the plunger to pass by the viewing port when the conax detonator is activated. This is illustrated in Fig. 16. The spectrometer windowless plunger design has been described in detail elsewhere, see Refs. 8-10. Basically the quick-acting plunger allows for a short term windowless coupling to the radiation that is detected and output by three separate channels or bare EMI photomultiplier tubes within the spectrometer. A micrometer adjustment on the spectrometer grating assembly permits wavelength selection within the instruments operating range.

Timing of the plunger open time is critical, since it was desirable to have the spectrometer viewing the shock front when it is within two or three feet of the endwall, and before shock reflection. Test firings of the detonator-plunger system were made to establish a timing sequence. Nominally the delay from the time the detonator is activated to the time the plunger aperture begins to slide by the port, in the endwall flange is $\sim 125\ \mu$ sec. Nominally, the window is open for 130 μ sec. These results are very repeatable and when combined with expected shock velocities, appropriate time delays were used to have the spectrometer open time coincide with the last two or three feet of shock travel down the tube. Timing could be such that the plunger closed just as the shock reflected off the endwall. This timing sequence is illustrated for a typical experiment in Fig. 17. All of the oscilloscopes were triggered from an upstream thin-film gauge. The upper three records represent the three spectrometer photomultipliers. The photon spikes are the measured signal and the width corresponds with the plunger open time. The lower trace on the bottom record originates from a photomultiplier looking in the visible region of the spectrum, which

is mounted on the leg of the spectrometer that couples the spectrometer to the shock tube, see Fig. 15. When the plunger opens, radiation is allowed to enter the phototube thus slowing the time when the spectrometer also sees radiation. From this trace, it is clearly seen that the plunger open time is about 130 μ sec. The upper trace on the lower record of Fig. 17 is from a red endwall detection system that is configured in the spectrometer flange, see Fig. 16. The system is designed to have a field of view that fills the inside diameter of the shock tube 6 feet upstream from the endwall. An EMI No. 95586 photomultiplier views 6560 Å radiation axially up the tube from the oncoming shock. This yields the steady trace shown in the upper trace of the bottom record of Fig. 9. In addition to providing 6600 Å endwall data as a function of shock velocity, this trace combined with the visible PMT trace shows when the plunger opened with respect to the position of the shock wave. For the data shown in Fig. 17, the scopes were triggered by thin film gauge #4, at the sidewall optics station, 6 feet upstream from the endwall of the tube. Thus a radiative flux history of the last 6 feet of shock front travel is shown in each trace. The red endwall data, for example, shows a constant level of radiation as the shock front approaches the endwall, with a sudden excursion as the shock reflects from the endflange. Calibration of this system is discussed in Appendix A. The visible photomultiplier record in the spectrometer clearly shows the plunge open time of 130 μsec, with the plunger closing just prior to shock reflection. The VUV flux data obtained during this open time is shown on the three upper data traces. For this shock-tube test, a micrometer grating sitting of 344.2 was used to the following wavelengths (with a first order bandpass of 32 Å):

τ_D = 344.2	1st Order	2nd Order	3rd Order
P. M. T. No. 1	955 Å	477.5 Å	318.3 Å
P. M. T. No. 2	1030 Å	515 Å	343.3 Å
P. M. T. No. 3	1472 Å	736 Å	490.6 Å

During the course of the test series, it was observed (see Fig. 17 for example), that a very small VUV signal was obtained from the spectrometer - windowless plunger combination, due to the relatively small wavelength bandpass, and the approximate 17,000 ft/sec upper shock

speed obtained. A modified endwall system was then employed to obtain VUV flux data for the shock velocity range investigated. This is illustrated schematically in Figure 18. It consists of an adapter housing to the shock tube which can be evacuated or put under positive helium pressure. For all tests it was kept under a vacuum after being purged three times prior to each experiment. The EMR phototube previously used for the incident VUV data was installed on this endflange housing. The system is designed to also have a field of view filling the 3-inch inside diameter of the shock tube at a distance of 6 feet upstream from the endwall. Again, the oscilloscope was triggered from station No. 4, 6 feet upstream from the endflange. A typical record is shown in the upper trace of Fig. 19. Since the plunger-window is not used for this endwall configuration, the oncoming VUV flux is obtained continuously for the last 6 feet of travel. This is seen as a level plateau as shown in the data trace, followed by large excursions as the shock reflects at the endwall. The lower record on Fig. 19, taken from another experiment, shows the similarity between the red endwall and VUV data traces. If absorption were significant in the VUV, (i.e. 1050-1800 Å as determined by the EMR-PMT), the VUV trace would not be a constant level, rather increase in signal as the shock nears the endwall and the absorbing path is decreased. The VUV flux data obtained with the endwall configuration shown in Fig. 18, indicated a constant level of radiation over the last 6 feet of travel.

It should be noted that a preliminary red endwall configuration was used during the early part of the test series while the spectrometer adapter flange was being modified for the final red endwall system just discussed and shown in Fig. 16. This preliminary red endwall system is shown schematically in Fig. 20. This system, which was mounted externally to the shock tube, was utilized to obtain shock-tube performance data, instrumentation delay times, and obtained red endwall data as a function of shock speed. It consisted of an EMI No. 9558 PMT and the 6560 Å filter, with optical components designed to yield a system 3-inch FOV at a distance 6 feet upstream from the endwall. A pyrometer, tungsten filament calibration setup is also illustrated.

Figure 21 shows the experimentally determined endwall flux dependency on incident shock strength. As in the preceding section, the data is normalized by the actual detector output for each system obtained at the lowest shock speed (14,000 ft/sec). Thus, the relative signal strength variation with oncoming shock front velocity can be observed. The red endwall data was obtained with the configuration shown in Fig. 16, while the VUV data was obtained with the EMR-PMT configuration shown in Fig. 18. The red endwall data indicates a variation of approximately a factor of 7 (as compared to the sidewall red data variation of about 10, see Fig. 11) over the shock velocity range. The VUV flux data indicated essentially no dependency on shock speed (i.e. a variation of only 30%) for this velocity range, which can be compared to a variation of 20-25 reported for sidewall peak-height, as discussed in Section II.2.2. The He purge-pump procedure for the PMT adapter was completed prior to each test; in addition, this adapter was continuously pumped during a shock-tube experiment. These procedures minimize the possibility of atmospheric absorption effects on the measurements. In addition, a rough calibration was obtained after each test, using a neon/mercury Pen-Ray lamp, that showed no relative change in the EMR-PMT system sensitivity during the program. Thus, the reason for the apparent lack of VUV flux dependency on shock velocity is yet to be determined.

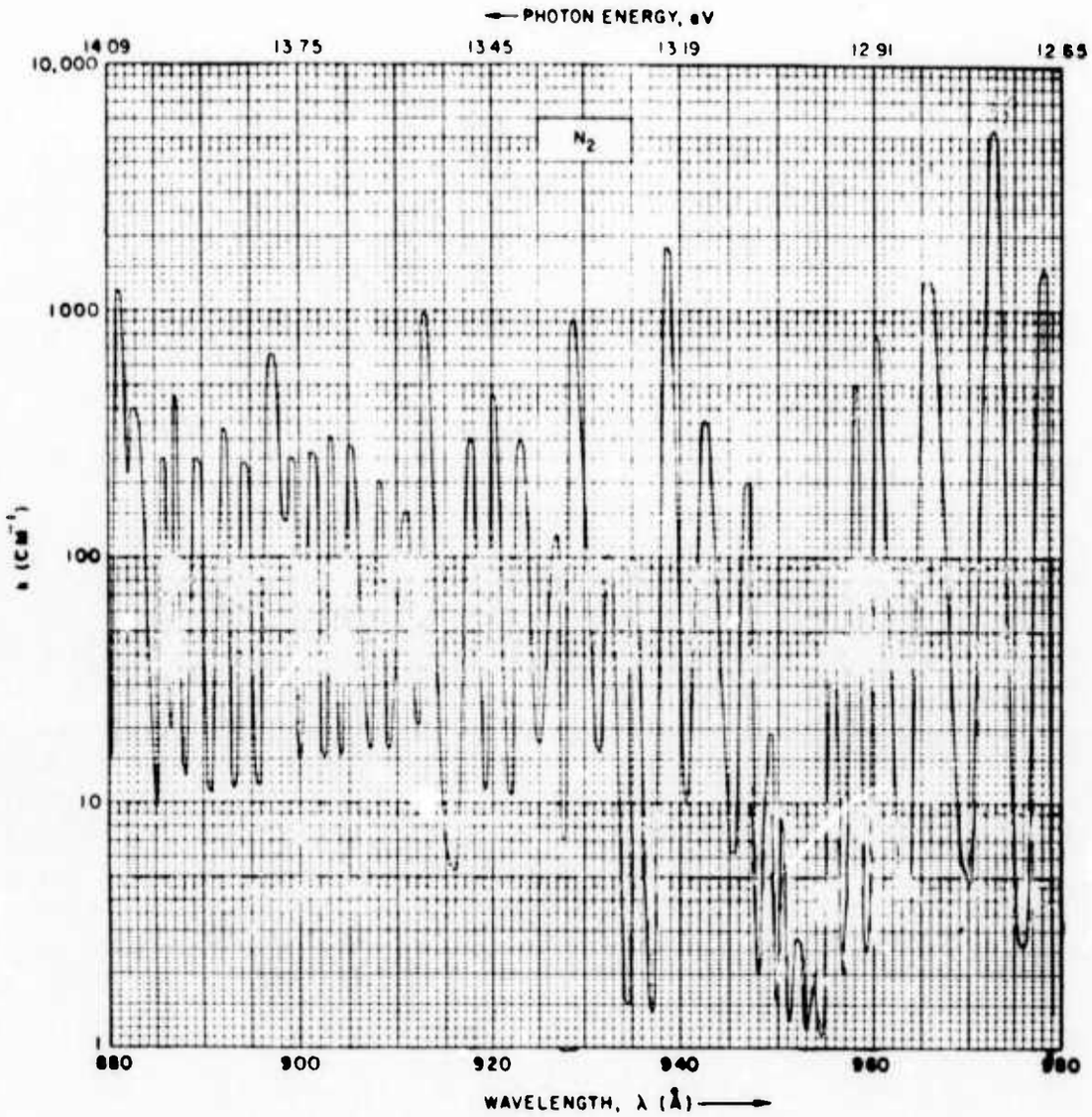

Figure 13. ABSORPTION AND PHOTOIONIZATION COEFFICIENT OF N_2

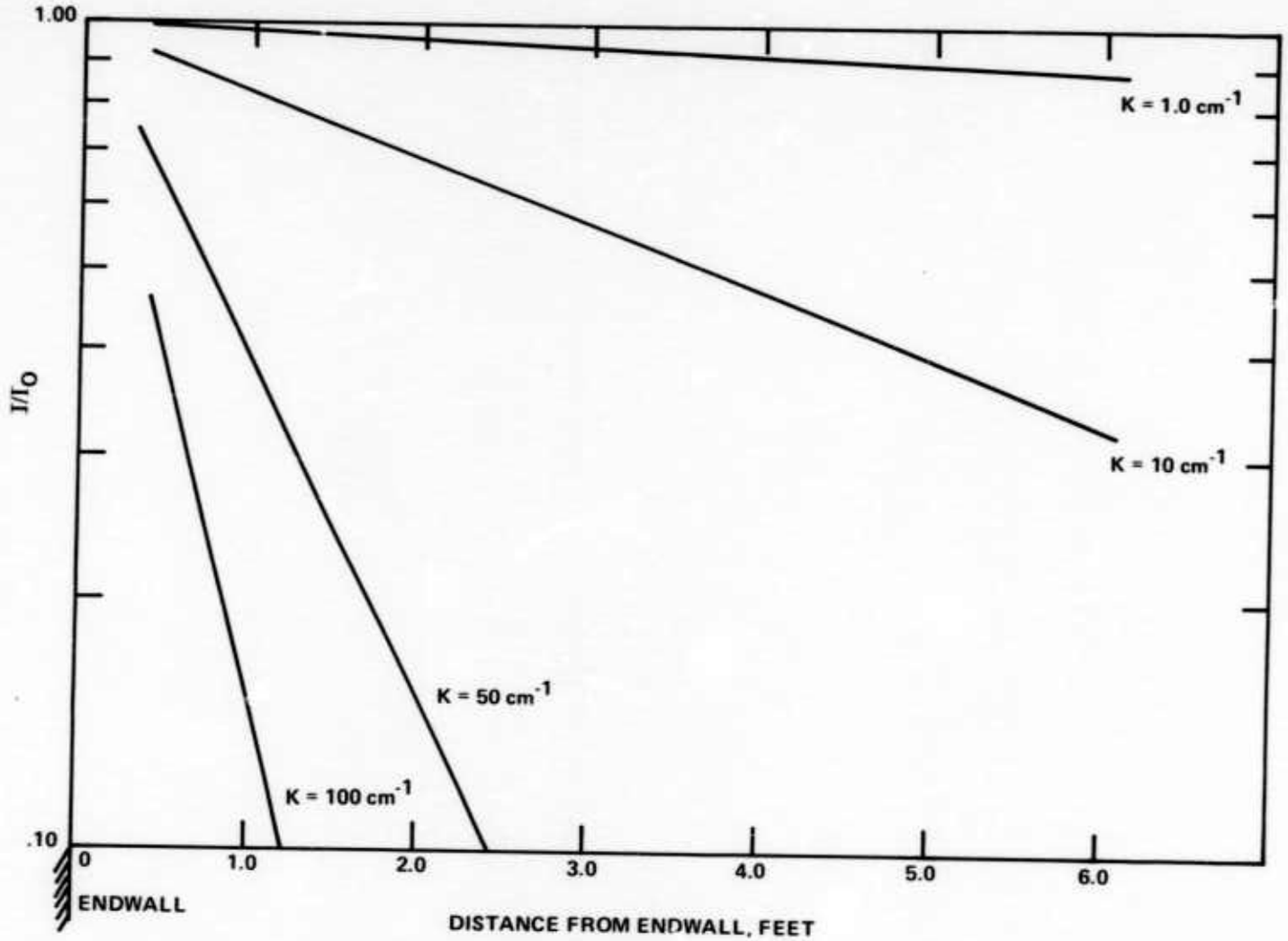

Figure 14 CALCULATED ABSORPTION AS FUNCTION OF DISTANCE FROM ENDWALL. P_1 = ½ TORR NITROGEN

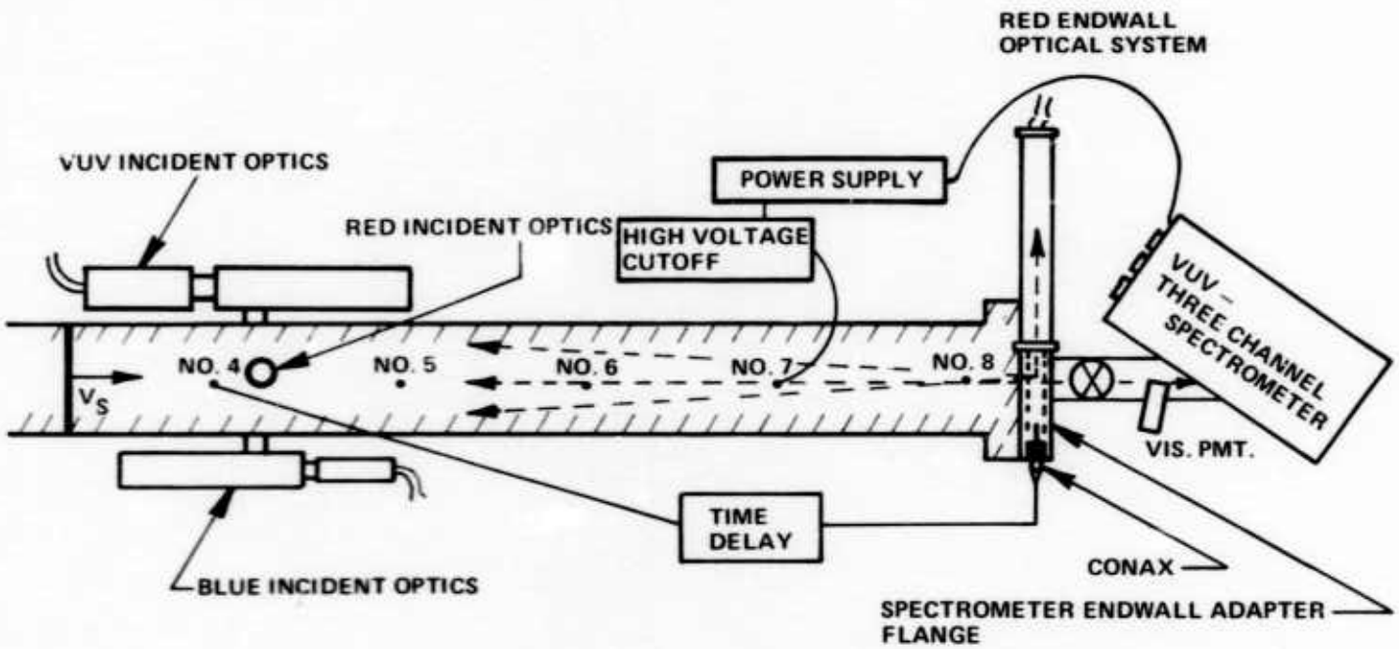

Figure 15 SCHEMATIC OF VUV - SPECTROMETER ENDWALL CONFIGURATION

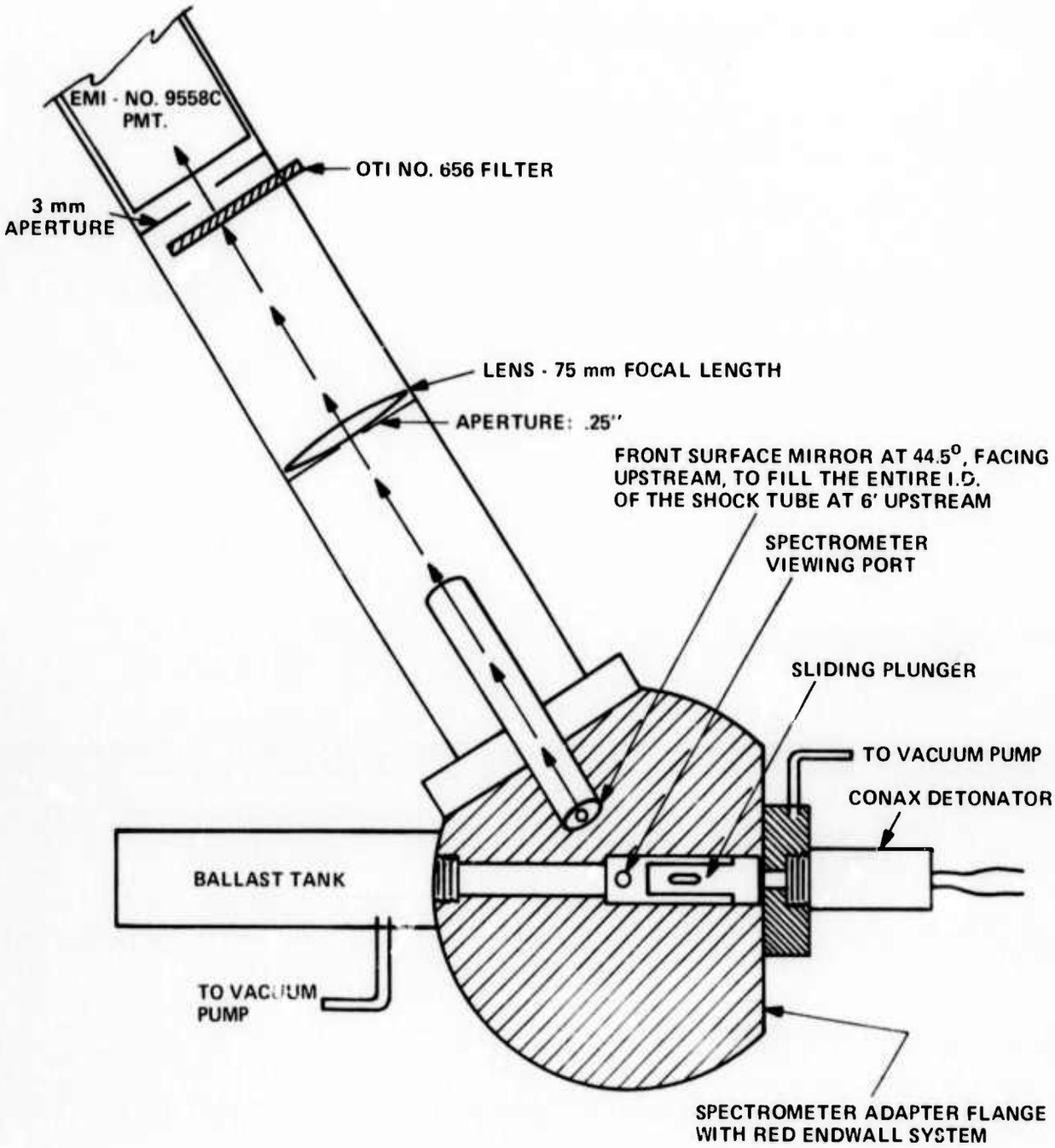

Figure 16 SCHEMATIC OF VUV - SPECTROMETER ENDWALL ADAPTER FLAGE WITH RED ENDWALL OPTICAL SYSTEM

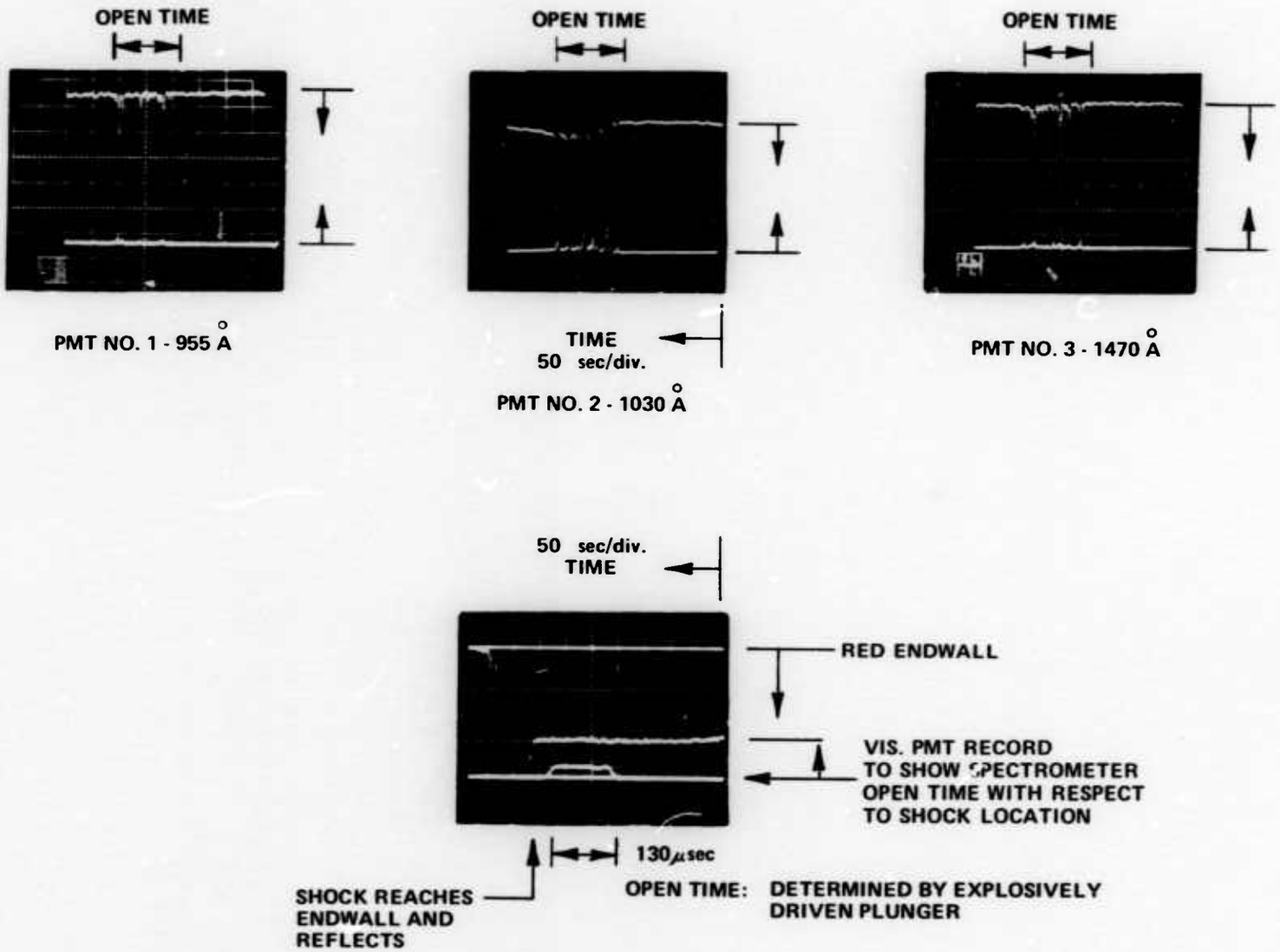

Figure 17 VUV SPECTROMETER ENDWALL DATA SHOWING PLUNGER TIMING.
$V_S \approx$ 16,500 ft/sec.: P_1 = ½ TORR NITROGEN

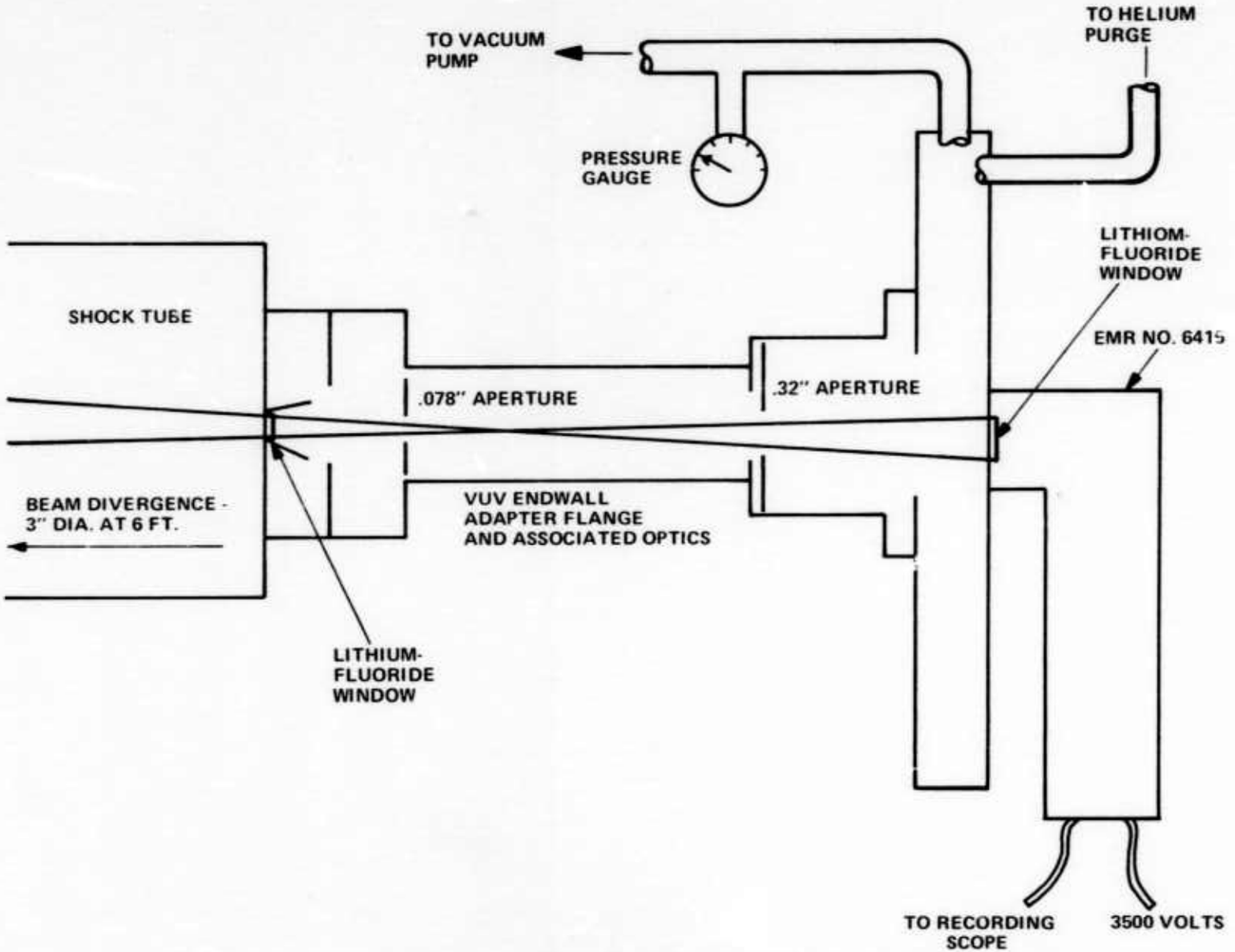

Figure 18 SCHEMATIC OF EMR-VUV PHOTOMULTIPLIER ENDWALL CONFIGURATION

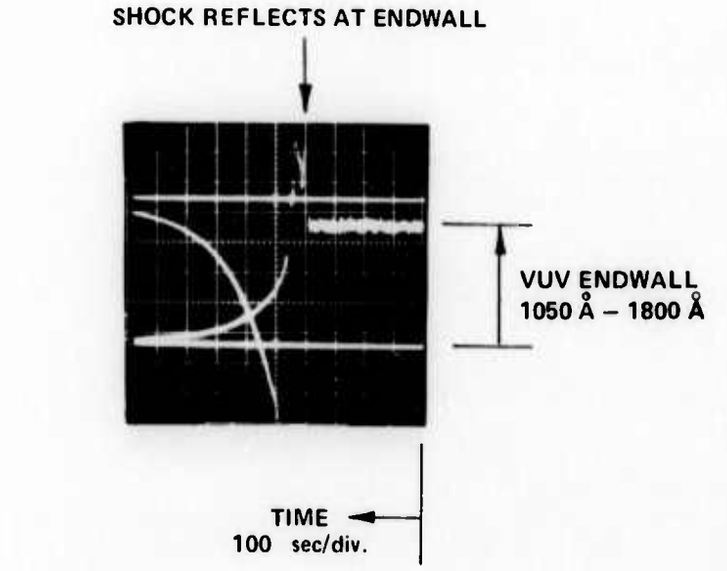

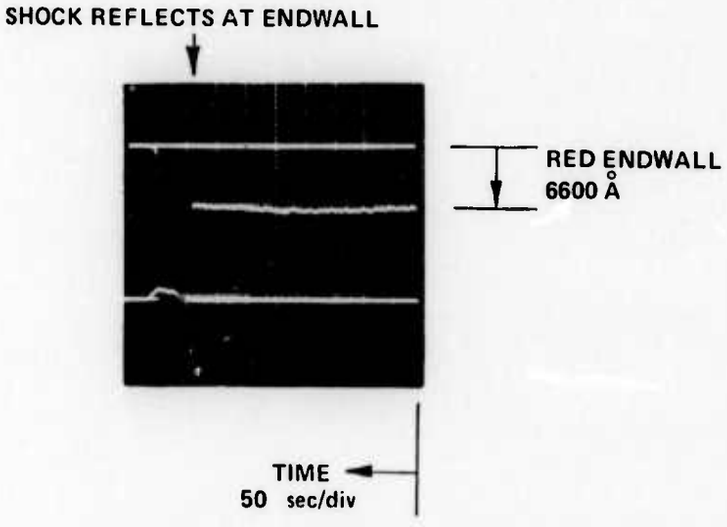

Figure 19 ENDWALL DATA FOR ONCOMING INCIDENT SHOCK RADIATION $V_S \approx$ 15,300 ft/sec.: P_1 = ½ TORR NITROGEN

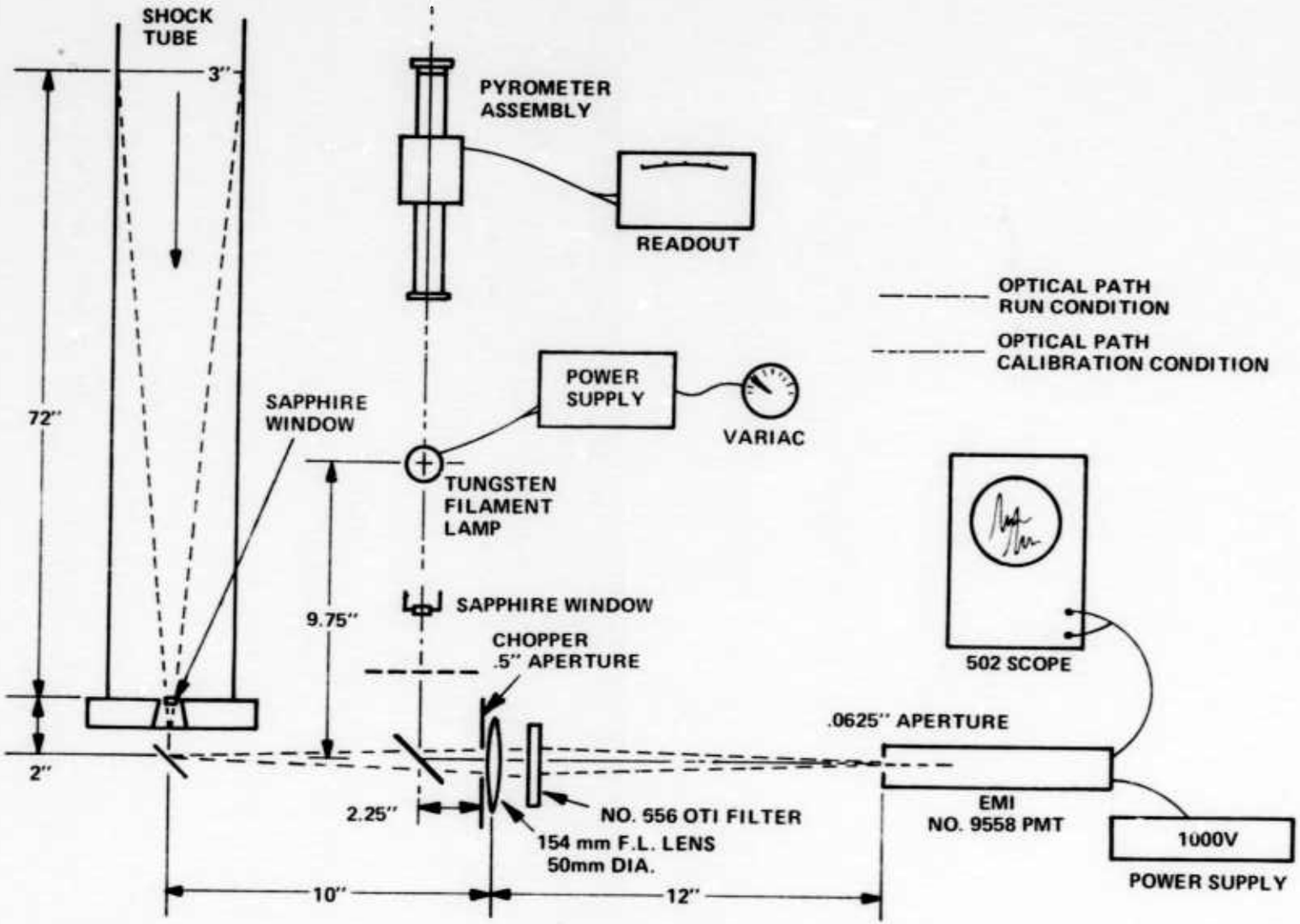

Figure 20 SCHEMATIC OF PRELIMINARY RED ENDWALL AND CALIBRATION CONFIGURATION

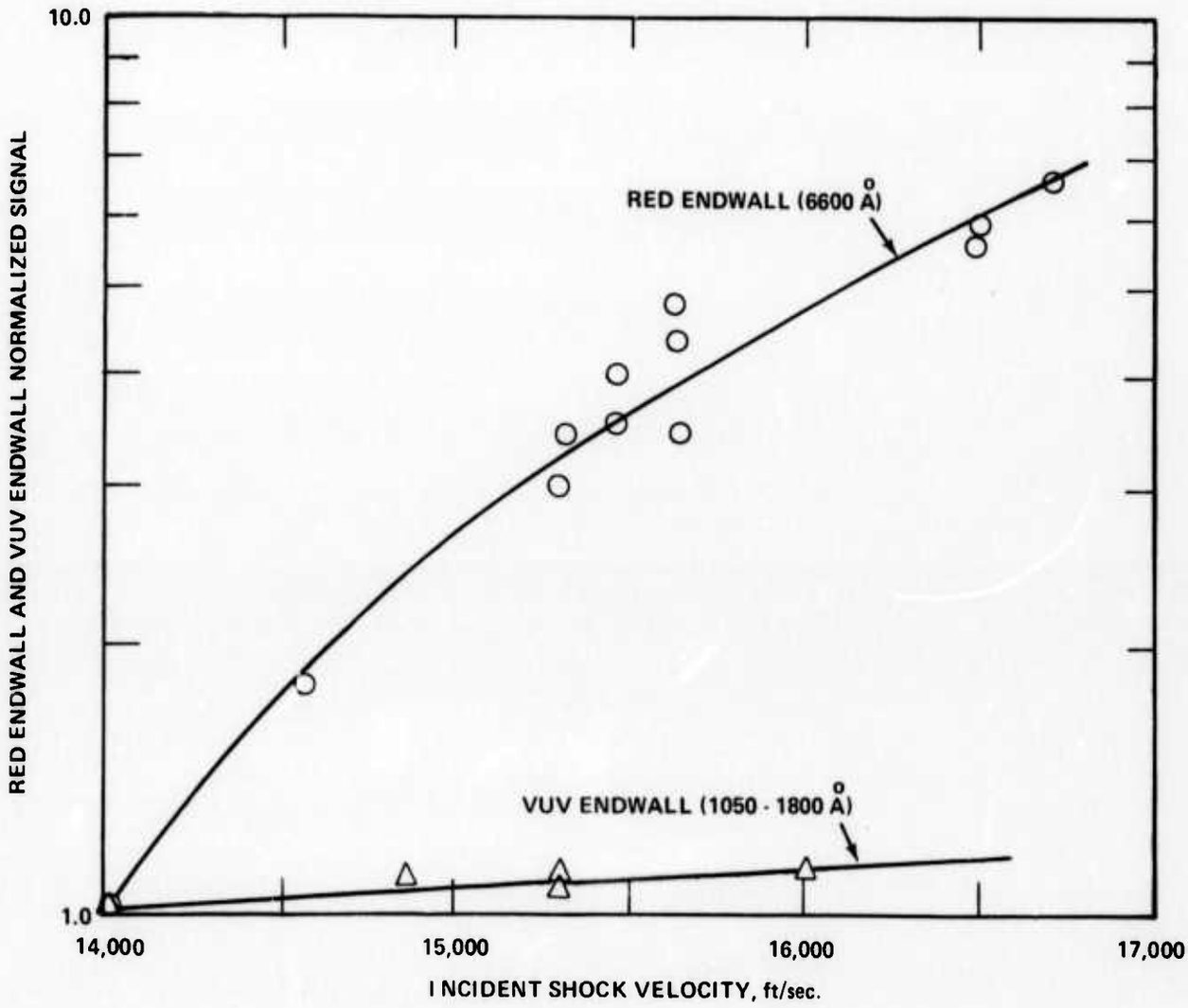

Figure 21 NORMALIZED RED AND VUV ENDWALL RADIATION DATA; P_1 = ½ TORR NITROGEN

III. SUMMARY

An experimental program to investigate basic vacuum ultraviolet photoionization processes in air has been completed at Calspan Corporation. Particular emphasis was directed toward the interaction of shock-induced non-equilibrium radiation with gaseous species. The experimental shock-tube program consisted of three main tasks:

1. Perform quantitative measurements to determine the contribution of the NO molecule to the nonequilibrium, vacuum ultraviolet emission spectrum from shock-heated air, (splitter-plate absorption measurements).
2. Investigate possible excitation mechanisms leading to VUV emission from molecular species pertinent to high-altitude rocket plume radiation, and shock-induced nonequilibrium, radiation, (sidewall radiation overshoot measurements).
3. Obtain quantitative, spectrally resolved measurements of the nonequilibrium, vacuum ultraviolet flux from advancing shock waves to verify previously developed excitation and radiative flux models, (endwall radiation measurements).

Experiments have been carried out pertinent to all three of the above tasks. The principal results for each are summarized below:

1. The splitter-plate absorption technique was utilized to investigate the role of NO in defining shock-induced vacuum ultraviolet radiative flux. Measurements using the splitter-plate technique for absorption in $N_2/O_2/N_e$ mixtures were obtained at selected wavelengths over a broad wavelength interval, 706 Å < λ < 1200 Å, at a resolution of $\Delta\lambda$ = 32 Å. The experimental data show substantial absorption at wavelengths of 812-980 Å. At 895 Å, for example, if the difference between the calculated and measured values of absorptance were attributed only to vibrationally excited NO, an absorption coefficient of $k_{NO} \approx 9,900\ cm^{-1}$ is obtained. This can be favorably compared with a measured value in cold NO of

approximately 9000 cm^{-1} at 898 Å. However, at the 812 Å and 970 Å wavelengths, if the indicated difference were ascribed only to NO, the absorption coefficients obtained are too high.

A discussion of this point is presented in the text, in which the role of strong O lines are shown to be critical to measurements at specific wavelengths. The results point out the need for careful analysis to evaluate both the presence and influence of all pertinent species in calculating the overall VUV properties of heated air.

2. Sidewall nonequilibrium overshoot measurements were obtained for pertinent radiating bands in nitrogen. Measurements were obtained in the red (6600 Å, N_2 1+ system), blue (2500 Å, N_2 4+ system) and VUV (1050-1800 Å) which showed very large nonequilibrium radiance levels close to the shock front for all three systems.

Values of the peak height as well as the time-to-peak were obtained for each band system as a function of shock velocity. For the well-known N_2(1+) system, for which an excitation model had been derived, the new data were shown to be in accord with earlier work. The data show that the (4+) system is excited more slowly than the (1+); on the other hand, the singlet states involved in VUV radiation are excited more rapidly than the N_2 (1+) triplet states.

The dependence of the VUV radiance on shock velocity was measured and documented in previous reports; the scope of the present program did not permit a detailed verification of the previous excitation model for the singlet-singlet VUV-emitting states.

3. A series of experiments was completed with new endwall diagnostics used to view radiation from advancing shock fronts. Measurements were obtained both in the VUV and red wavelength regions over a range of shock velocities in nitrogen. The 3-channel VUV spectrometer was attached to a new endwall flange in a windowless manner, utilizing

the explosively driven plunger. Advancing-shock VUV flux data were obtained for selected wavelength intervals, but the low flux level precluded quantative data analysis. More definitive VUV data were obtained over a larger bandpass (1050-1800 Å) using solar-blind photomultiplier tubes. Red (6600 Å, $N_2(1+)$ endwall data were also obtained with a refined diagnostic setup. The data indicated that the red endwall data showed a factor of approximately 7 increase over the velocity range similar to the factor of 10 increase obtained for the sidewall red overshoot peak variation. However, the VUV endwall data showed essentially no dependency on shock speed, when compared to an increase of a factor of 25 for the sidewall overshoot measurements.

No explanation for this result is available at present. Its resolution must await further experimentation with the apparatus modified to address this particular issue.

ACKNOWLEDGMENT

The authors wish to acknowledge the many and varied contributions of their colleague, the late John E. Stratton, whose creative experimental techniques were a major contribution to the research program. They also acknowledge the assistance of Mr. Robert Phibbs in the experimental phase of the work, Mr. Richard Hiemenz for the development of the electronic control systems, and Miss M. J. Williams for her assistance in obtaining the shock-computer program results.

REFERENCES

1. Edwards, K. R., Marrone, P. V., Olson, G. E. and Wurster, W. H The Photoionized Precursor Plasma and Its Effect on Blunt Body Radar Observables (U). Presented at the AIAA Joint Strategic Missile Sciences Meeting. U. S. Naval Academy, Annapolis, Maryland. 10-12 May, 1971 (SECRET).

2. Marrone, P. V. and Wurster, W. H.: Reentry Precursor Plasma-Determination of the Vacuum Ultraviolet Photoionizing Radiative Flux. Paper Presented at the 4th Entry Plasma Sheath Symposium. NASA Langley Research Center. October 13-15, 1970.

3. Precursor Ionization from Blunt Body Shock Waves: Annual Technical Report. Prepared by W. H. Wurster, Calspan Report No. AF-2581-A-2, July 1970.

4. Experimental Studies of Photoionization Processes in Air; Semi-annual Technical Report for Period 1 November 1971 to 1 May 1972. Calspan Report No. AI-3107-A-2, May 1972. Also Semi-annual Report for Period 1 May 1972 to 30 April 1973. Calspan Report No. AI-3107-A-3, April 1973, submitted by W. H. Wurster.

5. Watanabe, K., Matsunga, F. M. and Sakai, H.: Absorption Coefficient and Photoionization Yield of NO in the Region 580-1350 A. Applied Optics, Vol. 6, No. 3. March 1967. pp. 391-396.

6. Cook, G. R. and Ching, B. K.: Absorption, Photoionization, and Fluorescence of Some Gases of Importance in the Study of the Upper Atmosphere. Aerospace Corporation Report No. TDR-469(9260-01)-4. January 1965.

7. Watanabe, K., Marmo, F. F. and Inn, E.C.Y.: Photoionization Cross Section of Nitric Oxide. Physical Review, Vol. 91, 1953, p. 1155.

8. Marrone, P. V., Wurster, W. H. and Stratton, J. E.: Shock-Tube Studies of N^+ and O^+ Recombination Radiation in the Vacuum Ultraviolet. Calspan Report No. AG-1729-A-7. June 1968.

9. Marrone, P. V. and Stratton, J. E.: Vacuum Ultraviolet C^+ Recombination Radiation from Shock Heated CO/Ne Mixtures. Calspan Report No. RH-2786-A-1. March 1970.

10. Marrone, P. V. and Wurster, W. H.: Measurement of Atomic Nitrogen and Carbon Photoionization Cross Sections Using Shock Tube Vacuum Ultraviolet Spectroscopy. JQSRT, Vol. 11, No. 4 April 1971. 11. 327-349.

11. Williams, M. J. and Garr, L. J.: A Description of the Calspan Equilibrium Normal Shock Program. Calspan Internal Memorandum, September, 1966.

12. Wilson, K. H. and Nicolet, W. E.: Spectral Absorption Coefficients of Carbon, Nitrogen, and Oxygen Atoms. JQSRT. Vol. 7, No. 6. November/December 1967, pp. 891-943.

13. Wray, K. L. J. Chem. Phys. 44, 623, 1966.

14. Flagan, R. C. and Appleton, J. P. J. Chem. Phys, 56, 1163, 1972.

15. Wurster, W. H., Radiative Diagnostics in Nonequilibrium Flows, Modern Optical Methods in Gas Dynamic Research, edited by D. S. Dosanjh, Plenum Press, New York, pp 33-48, 1970.

APPENDIX A
CALIBRATION OF RED ENDWALL SYSTEM

A description is given of the calibration systems that were utilized to convert test data from the "spectrometer" red endwall system into standard units of radiance, watts - cm^{-2} - steradian^{-1} - micron. The conversion technique is discussed and the red endwall data obtained is presented in standard units of radiant intensity as a function of shock velocity.

The schematic below illustrates the apparatus used to calibrate the red endwall system:

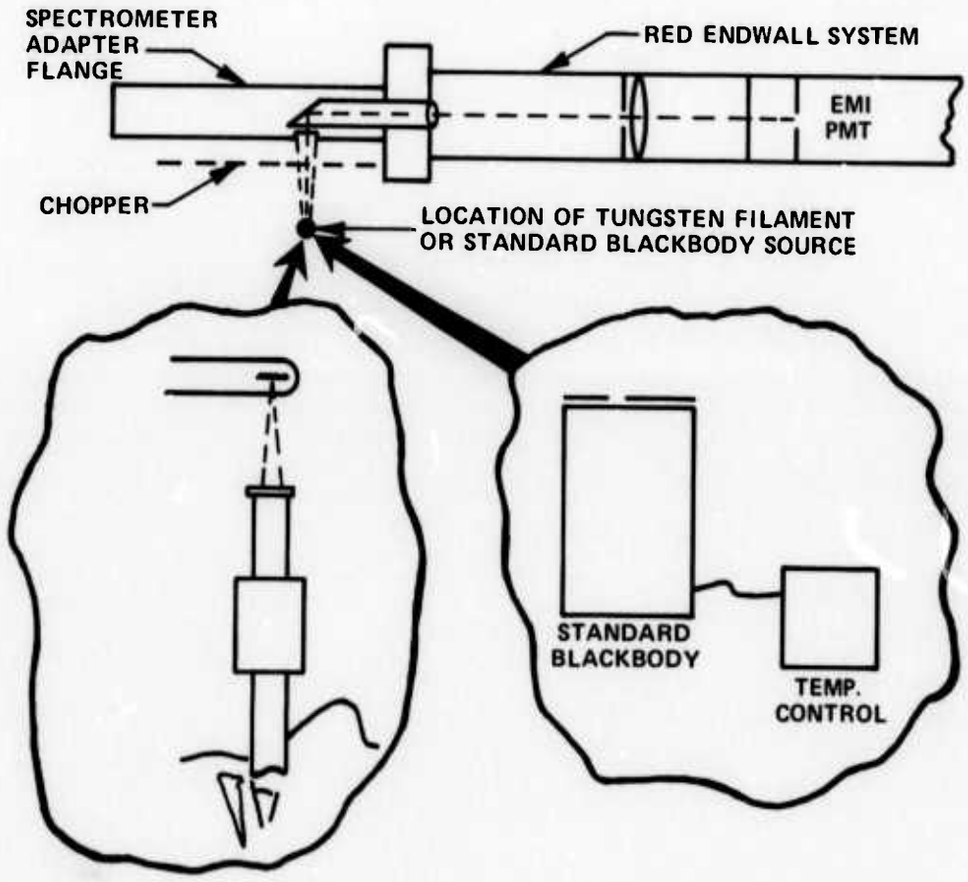

Figure 1A RED ENDWALL CALIBRATION SCHEMATIC

Initially a standard blackbody source was positioned in front of the window that allows radiation to enter the optical system, so as to fill the entire field of view of the endwall system. A chopper was inserted between the window and source and measurements were made of the systems response in millivolts as a function of source temperature. This result is plotted in Fig. 2A. To extend the range of the calibration so as to cover the range of signals obtained during the test series, a tungsten filament lamp-pyrometer calibration system was also used. The lamp was operated at several power settings while the signal from the red system was recorded and the tungsten filament temperature was determined with the pyrometer. The pyrometer measures the brightness temperature of the source. These results are also plotted in Fig. 2A. There is a slight discrepancy between the standard blackbody calibration and tungsten filament lamp calibration, over the range where a comparison can be made. This is attributed to a geometric factor in the calibration technique which is accounted for in the final analysis. The curves in Fig. 2A are then used in conjunction with the standard blackbody radiation tables to arrive at the calibration curve illustrated in Fig. 2B. The slope of this curve is calculated and used in the relationship,

$$I_{Test} = MV_{Test} \cdot \left(\frac{I_{BB}}{MV_{BB}}\right)_{Slope}$$

to calculate the radiant intensity from the advancing shock front as viewed by the endwall system. Using this relationship and the calibration results the red endwall data is presented in Fig. 3A in standard units of radiant intensity (watts - cm^{-2} - $steradian^{-1}$ - $micron^{-1}$) as a function at shock speed.

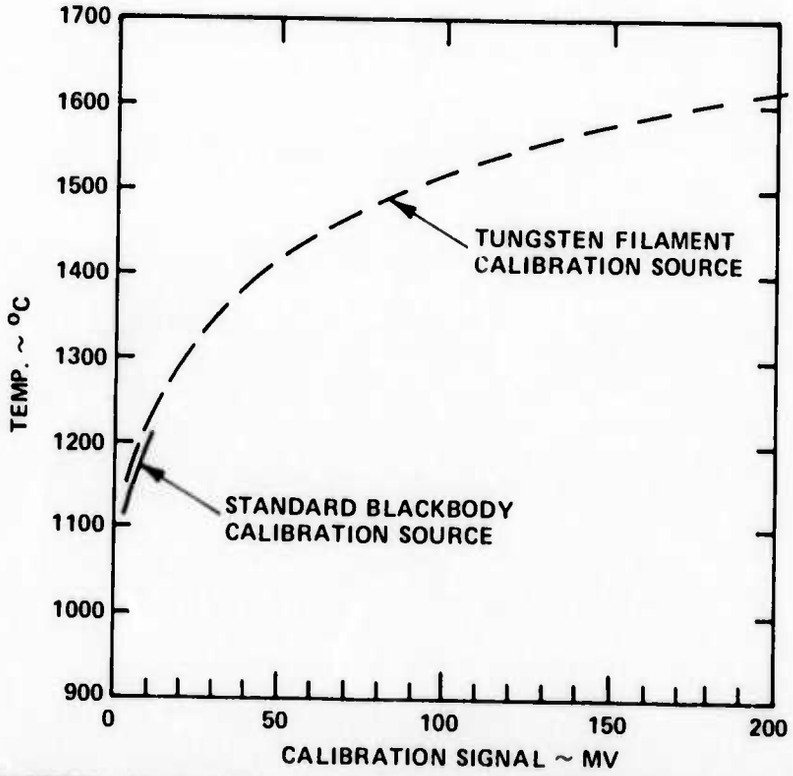

Figure 2A TUNGSTEN FILAMENT – BLACKBODY CALIBRATION DATA FOR THE RED ENDWALL SYSTEM

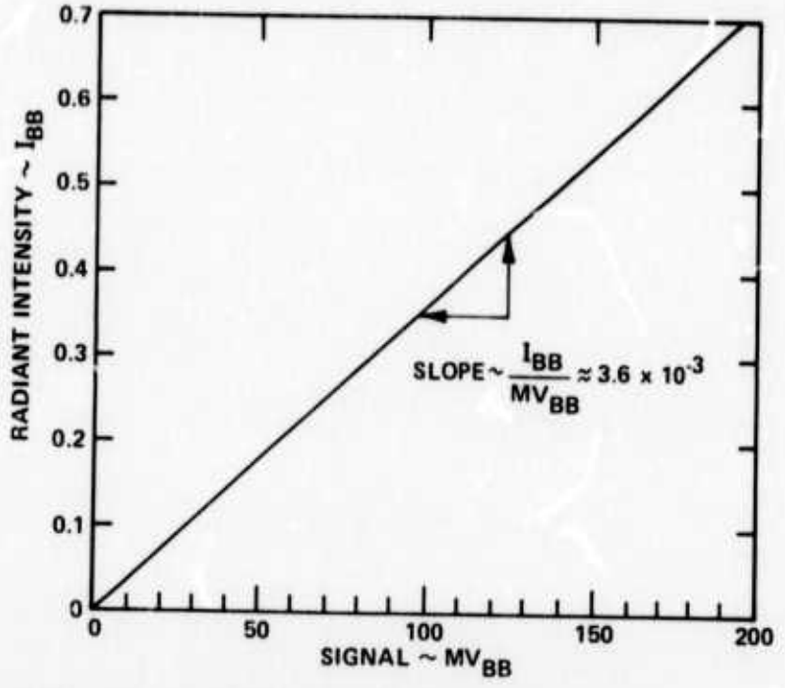

Figure 2B BLACKBODY CALIBRATION CURVE

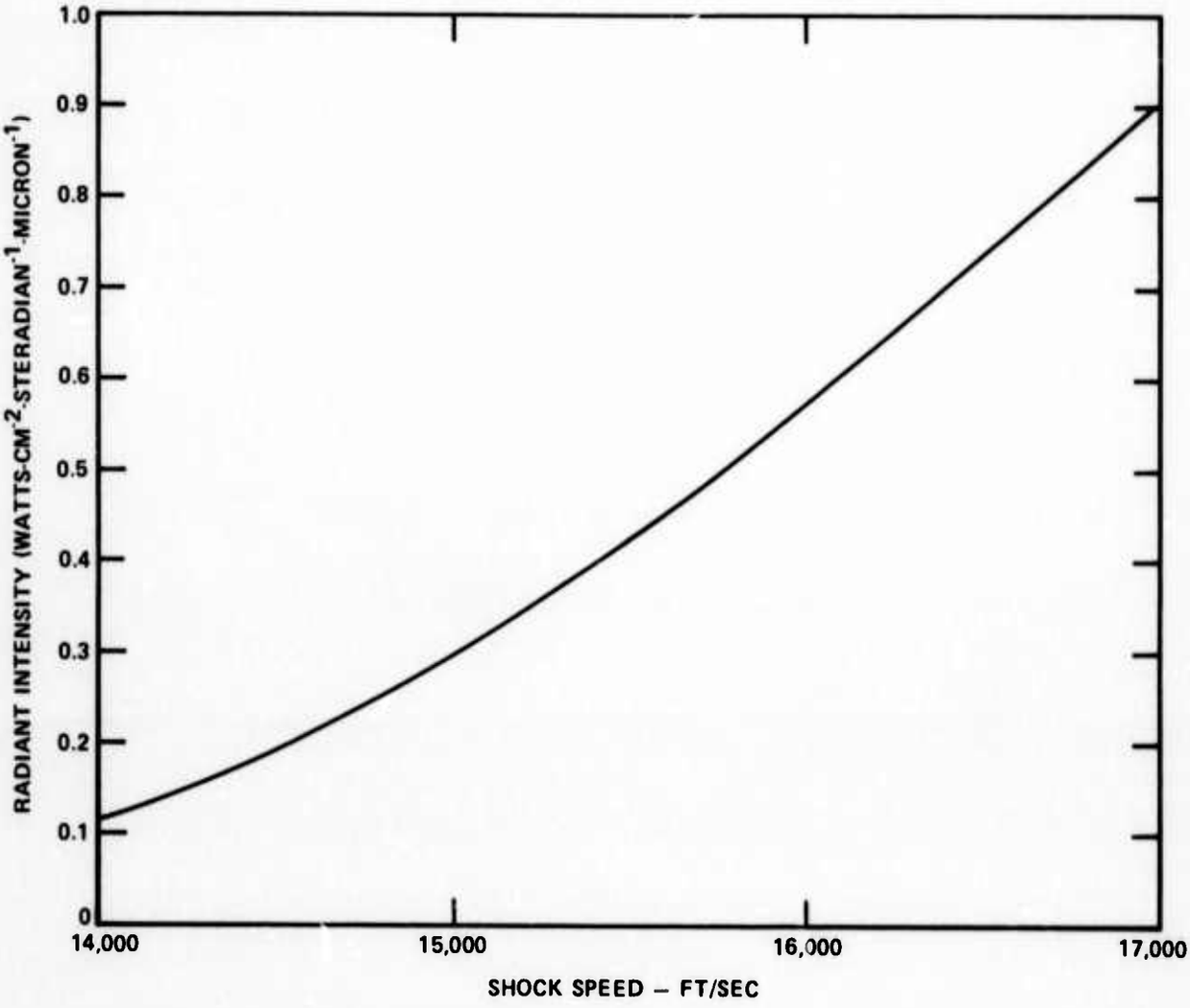

Figure 3A RADIANT INTENSITY OF THE ADVANCING SHOCK FRONT AS MEASURED BY THE RED ENDWALL SYSTEM